

Accepted by *The Astrophysical Journal*

Multifluid, Magnetohydrodynamic Shock Waves with Grain Dynamics II. Dust and the Critical Speed for C Shocks

Glenn E. Ciolek,^{1,2} Wayne G. Roberge,^{1,2} and Telemachos Ch. Mouschovias³

cioleg@rpi.edu, roberw@rpi.edu

ABSTRACT

This is the second in a series of papers on the effects of dust on multifluid, magnetohydrodynamic shock waves in weakly-ionized molecular gas. We investigate the influence of dust on the critical shock speed, v_{crit} , above which C shocks cease to exist. Chernoff showed that v_{crit} cannot exceed the grain magnetosound speed, V_{gms} , if dust grains are dynamically well coupled to the magnetic field. Since $V_{\text{gms}} \simeq 5 \text{ km s}^{-1}$ in a dense cloud or core, the potential implications for models of shock emission are profound. We present numerical simulations of steady shocks where the grains may be well- or poorly coupled to the field. We use a time-dependent, multifluid MHD code that models the plasma as a system of interacting fluids: neutral particles, ions, electrons, and various “dust fluids” comprised of grains with different sizes and charges. Our simulations include grain inertia and grain charge fluctuations but to highlight the essential physics we assume adiabatic flow, single-size grains, and neglect the effects of chemistry. We show that the existence of a phase speed v_ϕ does not necessarily mean that C shocks will form for all shock speeds v_s less than v_ϕ . When the grains are weakly coupled to the field, steady, adiabatic shocks resemble shocks with no dust: the transition to J type flow occurs at $v_{\text{crit}} \approx 2.76V_{\text{nA}}$, where V_{nA} is the neutral Alfvén speed, and steady shocks with $v_s > 2.76V_{\text{nA}}$ are J shocks with magnetic precursors in the ion-electron fluid. When the grains are strongly coupled to the field, $v_{\text{crit}} = \min(2.76V_{\text{nA}}, V_{\text{gms}})$. Shocks with $v_{\text{crit}} < v_s < V_{\text{gms}}$ have magnetic

¹New York Center for Studies on the Origin of Life (NSCORT)

²Department of Physics, Applied Physics and Astronomy, Rensselaer Polytechnic Institute, 110 8th Street, Troy, NY 12180

³Departments of Physics and Astronomy, University of Illinois at Urbana-Champaign, 1002 West Green Street, Urbana, IL 61801

precursors in the ion-electron-dust fluid. Shocks with $v_s > V_{\text{gms}}$ have no magnetic precursor in any fluid. We present time-dependent calculations to study the formation of steady multifluid shocks. The dynamics differ qualitatively depending on whether or not the grains and field are well coupled.

Subject headings: diffusion — dust, extinction — ISM: clouds — ISM: magnetic fields — MHD — plasmas — shock waves — waves

1. Introduction

Shock waves in weakly-ionized plasmas, such as the molecular outflows around young stellar objects, may have a multifluid structure, in which the charged and neutral components of the plasma behave as distinct fluids. If the shock speed is less than the speed with which the charged fluid communicates compressive disturbances, the charged particles are accelerated ahead of the neutral gas in a “magnetic precursor” (Mullan 1971; Draine 1980). The streaming of charged particles through the neutrals also accelerates, compresses and heats the neutral fluid. If it remains sufficiently cool, the neutral fluid is everywhere supersonic in a frame at rest in the post-shock gas. In this case all hydrodynamical variables are continuous and the entire structure is termed a “C shock” (Draine 1980). Alternatively the neutral fluid must undergo a transonic transition. This may occur smoothly via continuous flow through a sonic point (a “C* shock”, see Chernoff 1987 and Roberge & Draine 1990, but note that Chièze, Pineau des Forêts, & Flower 1998 question the reality of C* shocks) or abruptly at a viscous jump front (a “J shock”).

Simulations of the different types of multifluid MHD shocks reveal distinct observational signatures, including the strengths and velocity profiles of atomic and molecular emission lines (Chernoff, Hollenbach, & McKee 1982; Draine & Roberge 1982; Draine, Roberge, & Dalgarno 1983, henceforth DRD83; Smith & Brand 1990a,b; Smith 1991a,b; Smith, Brand, & Moorhouse 1991a,b; Kaufman & Neufeld 1996a,b; Timmermann 1996; Neufeld & Stone 1997; Pineau des Forêts et al. 2001), the ortho/para ratio of H_2 (Timmermann 1998, Wilgenbus et al. 2000), and the abundances of various chemical species in the post-shock gas (e.g., DRD83; Flower, Pineau des Forêts, & Hartquist 1985; Pineau des Forêts, Flower, & Dalgarno 1988; Flower & Pineau des Forêts 1994; Flower et al. 1996; Bergin, Neufeld, & Melnick 1998). When the simulations are used to model the rich array of spectral observations now available for molecular outflows, a combination of C- and J shocks is broadly satisfactory, but an acceptable explanation for important aspects of the observations remains elusive (e.g., Smith, Eislöffel, & Davis 1998; Rosenthal, Bertoldi, & Drapatz 2000). Consequently, the theory of multifluid shocks remains of considerable interest.

In this paper we reexamine a fundamental prediction of the theory, namely, the “critical speed,” v_{crit} , above which C type solutions fail to exist. According to most prior work, the transition from C- to J-type solutions occurs when the neutral flow becomes too hot to remain subsonic. For shocks in dense molecular gas, the transition is caused either by the onset of H_2 dissociation (which decreases radiative cooling of the neutral gas) or by self-ionization (which increases heating by ion-neutral scattering). The precise value of v_{crit} is sensitive to the rates of various atomic and molecular processes. DRD83 estimated that $49 \geq v_{\text{crit}} \geq 40 \text{ km s}^{-1}$ for preshock densities in the range $10^4 \leq n_{\text{H}} \leq 10^6 \text{ cm}^{-3}$. Analogous calculations by Smith (1994) give similar values, though recent simulations by Le Bourlot et al. (2002) predict somewhat larger critical speeds (e.g., $v_{\text{crit}} \approx 70 \text{ km s}^{-1}$ for $n_{\text{H}} = 10^4 \text{ cm}^{-3}$). In any case, shocks in dense molecular gas would be C type for speeds $\gtrsim 40\text{--}50 \text{ km s}^{-1}$ if the critical speed was determined solely by the temperature of the neutrals.

However v_{crit} is also constrained by the “signal speed” for compressive waves in the charged fluid, since shocks faster than the signal speed must necessarily be J type. In a cold, weakly-ionized molecular gas, $v_{\text{sig}} \simeq B/\sqrt{4\pi\rho_c}$, where B is the magnetic field strength and ρ_c is the mass density of charged particles. If ρ_c is taken to be the density of atomic and molecular ions, then $v_{\text{sig}} = V_{\text{iA}}$, where $V_{\text{iA}} \gtrsim 1000 \text{ km s}^{-1}$ is the ion Alfvén speed. In this view the constraint imposed by the signal speed would be of no practical significance. However dust grains are also (mostly) charged (e.g., see Fig. 1 of Paper I) and, to the extent that the grains are “loaded” onto the field lines, their contribution to ρ_c also should be included (McKee, Chernoff, & Hollenbach 1984). For example, if ρ_c is taken to be the *total* dust density, then $v_{\text{sig}} = V_{\text{gms}}$, where $V_{\text{gms}} \approx 5 \text{ km s}^{-1}$ (see eq. [28]) is the grain magnetosound speed. A critical speed this small would have profound implications for models of shocked molecular outflows. Flower & Pineau des Forêts (2003) have computed the abundance of charged grains in clouds including polycyclic aromatic hydrocarbons (PAHs) and cosmic-ray-induced UV photons. They suggest that only a small fraction of the total grain mass in a plasma containing PAHs is charged and coupled to the field, generally yielding magnetosound speeds $\sim 50 \text{ km s}^{-1}$. However, in the environments we wish to study, namely, dense, dark clouds and cores, it is likely that most PAHs have condensed or frozen onto the icy mantles of larger grains (Ehrenfreund & Charnley 2000; Bernstein et al. 2003; Gudipati & Allamondola 2003; Krügel 2003), and therefore should not affect the charge state of grains to such a large degree.

The critical speed v_{crit} would equal the grain magnetosound speed V_{gms} only if all the grains are well coupled to the magnetic field lines (Chernoff 1987). However, the grains may be only weakly coupled (e.g., Pilipp et al. 1990; Draine & McKee 1993) and grain charge fluctuations limit the effective mass of the loaded grains to some fraction of the total dust mass (Ciolek & Mouschovias 1993). Consequently, detailed numerical simulations

are generally required to determine v_{crit} . Although dust has been included in many detailed studies of shocks, most have neglected the inertia of the grains (i.e., the momentum equation for the dust has been omitted, on the assumption that the dust motion is force free). Because propagating waves in the grain fluid are suppressed when the grain inertia is neglected, studies of this type cannot be used to examine the connection between grain loading and v_{crit} .

In this paper we present numerical calculations which include the grain inertia, and extend Chernoff’s work by also including partial grain-field coupling and grain charge fluctuations. Our plan is as follows: In § 2 we summarize our assumptions and the free parameters in our models. The signal speed in a dusty plasma is discussed in § 3, where we examine the effects of dust on the phase velocities and damping rates of compressive waves. In § 4 we present numerical solutions for steady and time-dependent shock waves. Our results are summarized in § 5.

2. Modeling Assumptions and Parameters

We simulate time-dependent, MHD shock waves propagating in weakly-ionized plasmas using a finite difference code which is described in detail elsewhere (Ciolek & Roberge 2001, henceforth Paper I). We consider plane-parallel shocks propagating along the $\pm z$ direction of a Cartesian frame (x, y, z) . Fluid variables are assumed to depend only on z and time t . We restrict our discussion to “perpendicular shocks” with a magnetic field of the form $\mathbf{B} = B(z, t)\hat{\mathbf{x}}$. Fluid motions in the x -direction (i.e., along the magnetic field) are uncoupled from those in the y and z -directions and are ignored. Self gravity of the gas is also neglected.

Our code models the plasma as a system of up to nine interacting fluids: neutral particles (denoted by subscript n), electrons (e), ions (i), large dust grains (g^- , g^0 , and g^+) and very small grains or PAHs (sg^- , sg^0 , sg^+) with charges -1 , 0 , and $+1$ times the proton charge, e . The governing equations presented in Paper I are solved here for the special case of vanishing PAH or very small grain abundances since, as noted in the preceding section, they are likely to be depleted onto large grains in dense cores.

Our code has the capacity to include radiative cooling of the neutral gas by H_2 , CO , and H_2O molecules, as well as cooling by collision-induced dissociation of H_2 . For the calculations reported in this paper, however, we “turned off” the neutral cooling. The assumption of adiabatic flow was adopted for two reasons: First, the structure of a *steady* adiabatic shock with constant fractional ionization can be calculated exactly (Chernoff 1987; Smith & Brand 1990c), and this provides a valuable benchmark on our numerical results. Second, Chernoff (1987) showed that shocks in a weakly-ionized plasma undergo a C- to J-type transition at $v_{\text{crit}} = 2.76V_{\text{nA}}$, where $V_{\text{nA}} = B/\sqrt{4\pi\rho_n}$ is the neutral Alfvén speed. This conclusion

holds if (i) the charged particles are well coupled to the magnetic field and (ii) the shock is subAlfvénic in the charged fluid. Since these criteria are always satisfied by the ions, the occurrence of a C-J transition at any other critical speed, if found, can be attributed unambiguously to the effects of dust. With neutral cooling turned off, only the abundances of the major species H, H₂, and He (on which the “source terms” for energy and momentum transfer between the charged and neutral fluids depend; see Paper I) are required. We omit atomic hydrogen since the shocks considered here are too slow to be dissociative and fix the other abundances at $n(\text{H}_2) = 0.5n_{\text{H}}$ and $n(\text{He}) = 0.1n_{\text{H}}$.

The ion fluid is composed of generic atomic (subscript a⁺) and molecular (m⁺) ions with identical masses, $m_{\text{a}^+} = m_{\text{m}^+} = 25 \text{ amu}$. The ion abundances are described by a rudimentary chemical network which allows for changes in the fractional ionization caused by dissociative recombination, etc (see Paper I). In this paper we “turned off” the chemistry so that steady solutions could be calculated exactly. We neglected the inertia of the ions and electrons because they attain force-free motion on length scales that are many orders of magnitude smaller than the flow scale, and are therefore impractical to track with our finite difference scheme. Thermal pressure forces on the ions and electrons are negligible compared to electromagnetic forces and gas drag, and so were ignored. Because the heat capacities of the ion and electron fluids are small, their temperatures were calculated by requiring these fluids to be in thermal balance (see Chernoff 1987).

The large grains (henceforth simply “grains”) were assumed to be spherical with identical radii, a_{g} , and to be composed of material with density 3 g cm^{-3} . Realistic simulations with a spectrum of grain sizes will be presented elsewhere. Our purpose here is to elucidate the essential physics.

The free parameters in our calculations are listed in Table 1. Parameters that describe the undisturbed preshock plasma have realistic values for a typical cloud core, except that the cosmic ray ionization rate has been artificially adjusted so that all calculations have the same fractional ionization. We considered two simple dust models, in which the dust is either weakly coupled (the WC model) or strongly coupled (the SC model) to the magnetic field. Both models have a realistic dust-to-gas mass ratio, but the grain radii were chosen artificially to give large and small values for the grain Hall parameter,

$$\Gamma_{\text{g}} = \Omega_{\text{g}} \tau_{\text{drag}}^{(\text{g},\text{n})} , \quad (1)$$

where Ω_{g} is the charged-grain gyrofrequency and $\tau_{\text{drag}}^{(\text{g},\text{n})}$ is the grain-neutral collision time. We give values of Γ_{g} and other pertinent quantities in Table 2.

3. Compressive Disturbances in a Weakly Ionized, Dusty Plasma

3.1. Wave Modes

A weakly-ionized, dusty plasma supports a variety of waves with phase velocities and damping times that can be obtained by solving the appropriate dispersion relations. Pilipp et al. (1987, hereafter PHHM87) solved the dispersion relation for Alfvén (i.e., noncompressive) waves including the effects of partial field coupling and charge fluctuations. PHHM87 found that, when the grains are well coupled to the field lines, their added inertia reduces the phase velocity relative to a dust-free plasma that is otherwise identical. Ciolek & Mouschovias (1989, hereafter CM89) carried out the analogous calculations for waves propagating at an arbitrary direction relative to the field. Here we consider the special case of CM89’s analysis for the magnetosonic (i.e., compressive) modes relevant to the formation of magnetic precursors. Since some of the physics is both interesting and not published elsewhere, we describe the results in some detail.

We obtained the dispersion relation by linearizing the equations of motion about a uniform, static unperturbed state and searching for monochromatic plane-wave solutions of the form

$$q_1(z, t) = \tilde{q}_1(k) \exp[i(kz - \omega t)], \quad (2)$$

for the first-order perturbation q_1 in variable q . The perturbations were assumed to have the geometry appropriate for magnetosonic modes. We linearized the equations of motion from Paper I with several modifications: We omitted the equations of motion for very small grains on the assumption they are depleted (see §2). We omitted the continuity equations for the ions and grains because, for the very low fractional ionizations of interest here, their density perturbations have virtually no effect on the dynamics. We included the momentum equation for the ions (the ion inertia is neglected in Paper I and in our numerical code) since otherwise waves in the ion fluid would be suppressed. We assumed for simplicity that the perturbations are adiabatic, and therefore omitted the energy equation for the neutral fluid. Finally, in writing the magnetic induction equation we assumed that magnetic flux is frozen into the electron fluid. This is more general than the corresponding assumption in Paper I (flux freezing in the ion fluid) though equivalent in the limit of vanishing small grain abundance. Our results for the WC and SC models are shown in Figures 1 and 2, respectively, where $v_\phi \equiv \text{Re}[\omega]/k$ is the phase velocity and $\tau_{\text{damp}} \equiv -1/\text{Im}[\omega]$ is the damping time. Several wave modes are apparent.

3.1.1. Ion Magnetosound Waves and Quasiparticle Oscillations

At very short wavelengths only the ions and electrons are coupled to the magnetic field. In the ion magnetosound mode (labeled “ims” in Fig. 1-2), the ions, electrons and magnetic field oscillate against a background of fixed neutrals and grains. The phase velocity is the ion magnetosound speed,

$$V_{\text{ims}} \simeq V_{\text{iA}} = \frac{B}{\sqrt{4\pi\rho_{\text{i}}}}, \quad (3)$$

where $V_{\text{ims}} \simeq V_{\text{iA}}$ because we have neglected thermal pressure of the ions. For the core conditions adopted here, $V_{\text{ims}} \sim 1000 \text{ km s}^{-1}$ (Table 3).

Ion magnetosound waves do not exist for wavelengths larger than some value $\lambda_{\text{max}}^{(\text{ims})}$. In the WC model, $\lambda_{\text{max}}^{(\text{ims})}$ is the familiar cutoff imposed by ion-neutral friction,

$$\lambda_{\text{max}}^{(\text{ims})} = 4\pi V_{\text{ims}} \tau_{\text{drag}}^{(\text{i,n})} \quad (\text{WC model}) \quad (4)$$

(e.g., Kulsrud & Pearce 1969), where $\tau_{\text{drag}}^{(\text{i,n})}$ is the ion-neutral drag time.¹ In the SC model, the cutoff for ion magnetosound waves is the *electrostatic wavelength*,

$$\lambda_{\text{max}}^{(\text{ims})} = \lambda_{\text{elect}} \simeq \frac{2\pi V_{\text{ims}}}{\Omega_{\text{qp}}} \quad (\text{SC model}). \quad (5)$$

For $\lambda \geq \lambda_{\text{elect}}$ the ion magnetosound mode transforms into a nonpropagating² “quasiparticle” mode (labeled “qp” in Fig. 1-2).³ In the presence of charged grains, the ions and electrons collectively form a single “quasiparticle fluid” of electron-shielded ions with effective charge

$$Q_{\text{eff}} = \left(\frac{n_{\text{i}} - n_{\text{e}}}{n_{\text{e}}} \right) e \simeq \left(\frac{n_{\text{g}^-}}{n_{\text{e}}} \right) e. \quad (6)$$

The ions and electrons gyrate about the field lines at a constant frequency

$$\Omega_{\text{qp}} = \left(\frac{n_{\text{i}} - n_{\text{e}}}{n_{\text{e}}} \right) \Omega_{\text{i}} = \left(\frac{n_{\text{g}^-} - n_{\text{g}^+}}{n_{\text{e}}} \right) \Omega_{\text{i}} \simeq \left(\frac{n_{\text{g}^-}}{n_{\text{e}}} \right) \Omega_{\text{i}}, \quad (7)$$

¹In general, $\tau_{\text{drag}}^{(\text{i,j})}$ denotes the drag time for particles of type i to be slowed by elastic scattering with particles of type j, and $\tau_{\text{drag}}^{(\text{i,tot})}$ denotes the drag time for particles of type i to be slowed by scattering with all other particle types.

²Note that $d(\log v_{\phi})/d(\log \lambda) = 1$ on the branch labeled “qp”.

³The quasiparticle mode also appears in the WC model (Fig. 1). However, quasiparticle effects are insignificant in the WC model: the abundance of charged grains, and hence Q_{eff} , are ≈ 60 times smaller than in the SC model (see Table 2). As a result, Ω_{qp} is so small that the quasiparticle oscillations are evanescent.

where $\Omega_i = eB/m_i c$ is the ion gyrofrequency. For detailed discussions on the physics of quasiparticle oscillations, see Ciolek & Mouschovias (1993, 1994, 1995).

In both models, propagating ion magnetosound waves are damped by ion-neutral drag on a time scale

$$\tau_{\text{damp}}^{(\text{ims})} = 2\tau_{\text{drag}}^{(\text{i,n})}, \quad (\lambda < \lambda_{\text{max}}^{(\text{ims})}), \quad (8)$$

where the factor of 2 occurs because of equipartition between the kinetic and magnetic field energies. For $\lambda > \lambda_{\text{max}}^{(\text{ims})}$ ion-magnetosound waves are evanescent: the ions and magnetic field diffuse through the rest of the plasma with damping on the diffusion time scale,

$$\tau_{\text{damp}}^{(\text{ims})} = \frac{\lambda^2}{\pi V_{\text{ims}} \lambda_{\text{max}}^{(\text{ims})}} \quad (\lambda > \lambda_{\text{max}}^{(\text{ims})}). \quad (9)$$

3.1.2. Grain Magnetosound Waves

At somewhat larger wavelengths, grains participate in the wave motions provided they are coupled to the magnetic field. Thus, grain magnetosound waves (labeled “gms”) appear in the SC model but not in the WC model. In the former, g^- and g^+ grains are directly attached to the field lines and the neutral grains are effectively attached by charge fluctuations.⁴ Accordingly, ions, electrons and dust all contribute to the inertia of the wave and the phase velocity is the grain magnetosound speed,

$$V_{\text{gms}} = \frac{B}{\sqrt{4\pi (\rho_i + \rho_e + \rho_g)}}, \quad (10)$$

where ρ_g is the total density of charged and uncharged dust. Because the dust density is much larger than the ion density, the grain magnetosound speed is much smaller than the ion magnetosound speed ($V_{\text{gms}} \ll V_{\text{ims}}$, see Table 3).

Grain magnetosound waves are allowed for wavelengths larger than

$$\lambda_{\text{min}}^{(\text{gms})} \simeq \frac{\pi V_{g^- \text{ms}}}{\Omega_{\text{qp}} \tau_{\text{drag}}^{(\text{i,n})} \cdot \Omega_g}, \quad (11)$$

where $V_{g^- \text{ms}}$ ($\simeq V_{\text{gms}}$, since $n_{g^-} \gg n_{g^0}$, n_{g^+} — see Table 2) is the magnetosound speed in the fluid of *charged* grains and Ω_g is the grain gyrofrequency. The minimum wavelength

⁴Attachment of the neutral grains occurs if the time for a neutral grain to capture an electron or ion is much less than the g^0 -neutral drag time, $\tau_{\text{drag}}^{(g^0, \text{n})}$ (PHHM87; CM89; Ciolek & Mouschovias 1993). This inequality is satisfied by the SC and “intermediately-coupled” IC (see § 4.2.1) models.

$\lambda_{\min}^{(\text{gms})}$ signifies some interesting and unique plasma physics: propagation of magnetosound waves in the grain fluids is aided by an electrostatic attraction between the positively-charged quasiparticles and the negatively charged grains (CM89). For $\lambda \geq \lambda_{\min}^{(\text{gms})}$, the electrostatic attraction between the quasiparticles and charged grains allows the charged grains to be “dragged along” with the magnetically attached quasiparticles and the field (see Ciolek & Mouschovias 1993, § 3.1.2). The maximum wavelength for grain magnetosound waves is determined by gas-grain friction. The cutoff occurs at

$$\lambda_{\max}^{(\text{gms})} = \frac{4\pi V_{\text{gms}} \tau_{\text{drag}}^{(\text{g,n})}}{1 + \left[(\rho_{\text{i}}/\rho_{\text{g}}) \left(\tau_{\text{drag}}^{(\text{g,n})} / \tau_{\text{drag}}^{(\text{i,n})} \right) \right]} \quad (12)$$

(CM89). For $\lambda > \lambda_{\max}^{(\text{gms})}$, the waves are evanescent and the combined plasma of ions, electrons and dust diffuses relative to neutrals.

At small wavelengths (i.e., $\lambda \sim \lambda_{\min}^{(\text{gms})}$), grain magnetosound waves are damped primarily by the drift of quasiparticles and magnetic field relative to the charged grains. The damping time is

$$\tau_{\text{damp}}^{(\text{gms})} \simeq \frac{1}{2\pi} \frac{\lambda^2}{\lambda_{\min}^{(\text{gms})} V_{\text{g-ms}}} \quad \text{if } \lambda \sim \lambda_{\min}^{(\text{gms})} \quad (13)$$

and this “damping branch” therefore has a slope $d \log \tau_{\text{damp}} / d \log \lambda = 2$ in Fig. 2*b*. At longer wavelengths the diffusion of quasiparticles with respect to grains is significantly lessened and the waves are damped by the frictional drag on the grains and ions exerted by the neutrals (which are essentially motionless at these frequencies). In this regime the damping timescale becomes independent of λ and the damping curve in Fig. 2*b* flattens. The damping rate is the sum of the damping rates for ion-neutral and grain-neutral friction, so that

$$\tau_{\text{damp}}^{(\text{gms})} \simeq 2 \left\{ \left[\frac{\rho_{\text{i}}/\rho_{\text{g}}}{\tau_{\text{drag}}^{(\text{i,n})}} \right] + \left[\frac{1}{\tau_{\text{drag}}^{(\text{g,n})}} \right] \right\}^{-1} \quad \text{if } \lambda_{\min}^{(\text{gms})} \ll \lambda \leq \lambda_{\max}^{(\text{gms})}, \quad (14)$$

where

$$\frac{1}{\tau_{\text{drag}}^{(\text{g,n})}} \equiv \sum_{\delta} \frac{\rho_{\text{g}}^{\delta}}{\rho_{\text{g}} \tau_{\text{drag}}^{\text{g},\text{n},\delta}}. \quad (15)$$

and the factor of 2 again appears because of equipartition between the kinetic and magnetic field energies in the wave. For $\lambda > \lambda_{\max}^{(\text{gms})}$ the (evanescent) waves are damped on the diffusion time, with

$$\tau_{\text{damp}}^{(\text{gms})} \simeq \frac{\lambda^2}{V_{\text{gms}} \lambda_{\max}^{(\text{gms})}} \quad \text{if } \lambda > \lambda_{\max}^{(\text{gms})}. \quad (16)$$

3.1.3. Neutral Sound and Magnetosound Waves

Oscillations of the neutral fluid occur for all wavelengths. At small wavelengths, adiabatic neutral sound waves (labeled “ns”) occur wherein the neutrals oscillate in a sea of fixed ions and grains. The phase velocity is the adiabatic sound speed,

$$C_{\text{ad}} = \gamma^{1/2} C_{\text{n}} \simeq \left(\frac{5k_{\text{B}}T_{\text{n}}}{3m_{\text{n}}} \right)^{1/2}, \quad (17)$$

where γ is the adiabatic index of the gas (Table 3). Sound waves in the neutral fluid are damped by collisions between neutrals and the other fluids, so that

$$\tau_{\text{damp}}^{(\text{ns})} = 2 \left[\sum_{\alpha} \left(\frac{1}{\tau_{\text{n},\alpha}^{\text{d}}} \right) \right]^{-1}. \quad (18)$$

At longer wavelengths the ions and grains excite neutral magnetosound waves (labeled “nms”) consisting of longitudinal compressions of the bulk fluid (i.e., the neutrals plus the electron-ion-grain plasma) and magnetic field. The phase velocity is the neutral magnetosound speed,

$$V_{\text{nms}} = (C_{\text{ad}}^2 + V_{\text{nA}}^2)^{1/2}, \quad (19)$$

(Table 3). Since the neutral fluid density far exceeds the combined densities of all other fluids, the inertial response of the wave is almost entirely due to the neutrals. Thermal-pressure and magnetic forces — the latter affecting the neutral fluid indirectly through collisions between neutrals and charged particles — provide the restoring force required for wave propagation.

Propagation of neutral magnetosound waves becomes possible for wavelengths greater than the *minimum neutral magnetosound wavelength*,

$$\lambda_{\text{min}}^{(\text{nms})} = \pi \left(\frac{V_{\text{nA}}^2}{V_{\text{nms}}^2} \right) \tau_{\text{drag}}^{(\text{n,tot})} \quad (20)$$

(CM89). Note that for $V_{\text{nA}} \gg C_{\text{ad}}$, $(v_{\text{nA}}^2/V_{\text{nms}}^2) \rightarrow V_{\text{nA}}^2$. The minimum neutral magnetosound wavelength is the perpendicular ($\mathbf{k} \perp \mathbf{B}$) analog to the lower cutoff wavelength for neutral Alfvén waves ($\mathbf{k} \parallel \mathbf{B}$) in ion-neutral (Kulsrud & Pearce 1969) and dusty (PHHM87) plasmas. The damping of neutral magnetosound waves is due to ambipolar diffusion of the plasma and magnetic field with respect to the neutrals, with

$$\tau_{\text{damp}}^{(\text{nms})} = \frac{\lambda^2}{2\pi^2 V_{\text{nA}}^2 \tau_{\text{drag}}^{(\text{n,tot})}} \quad (21)$$

(see Fig. 1b,2b). For $\lambda > \lambda_{\text{min}}^{(\text{nms})}$ there also exists a non-propagating ($|v_{\phi}| = 0$) thermal-pressure-driven diffusion mode, in which the neutrals diffuse relative to a fixed background of plasma and magnetic field, which has $\tau_{\text{damp}} = \lambda^2/4\pi^2 C_{\text{n}}^2 \tau_{\text{drag}}^{(\text{n,tot})}$.

3.2. Propagation of Small-Amplitude Disturbances

The preceding section shows that disturbances in a dusty plasma can excite a variety of waves, with phase velocities and damping rates that span several orders of magnitude. We are ultimately interested in how compressive waves in the charged fluids affect the formation of C shocks, and we do this in §4 by simulating large-amplitude disturbances (i.e., shocks). However, it is instructive to consider first a simpler problem, the propagation of small-amplitude, Gaussian wave packets, where interpretation of the dynamics in terms of different modes is much simpler: the narrow range of length scales in such a packet limits the number of modes that are excited, and the linearity of the disturbance allows us to interpret the results using §3.1.

At time $t = 0$ we superimposed a perturbation

$$B(z) = \delta B \exp \left[-\frac{(z - Z/2)^2}{\ell_B^2} \right] \quad (22)$$

on a static, uniform initial state corresponding to either the WC or SC model. We centered the pulse initially on a computational domain $[0, Z]$ and followed its evolution with our numerical code. The code uses transmissive boundary conditions, which allow the pulse to exit the domain freely, i.e., without generating reflected pulses at the boundaries. Thus, the pulse should evolve exactly like an identical pulse in an infinite computational domain. In all cases we set $\delta B/B_0 = 0.1$ but chose a few different values of the packet width, ℓ_B .

Simulations of a wave packet with $\ell_B = 4 \times 10^{14}$ cm are described in Figure 3 for the WC model, where the left-hand panel shows fluid velocities and the right-hand panel shows the density and magnetic field. The upper and lower boxes show variables at times $t_1 = 8.5$ yr and $t_2 = 17$ yr, respectively. These times are so short ($t_1, t_2 \ll \tau_{\text{drag}}^{(n,i)}$, see Table 2) that the neutrals are virtually stationary. The grains, which receive their “marching orders” in the WC model mainly by colliding with the neutrals, are also motionless. The ions are not stationary, but the initial disturbance does not propagate: the “wave” packet simply sits at the center of the grid and decays away. The ions in Fig. 3 are diffusing through the grains and neutrals at the terminal drift speed determined by the balance between ion-neutral drag and the driving magnetic pressure gradient. The absence of wavelike (i.e., oscillatory) motions may seem surprising, since propagating ion magnetosound waves are permitted by the dispersion relation on the length scales $\sim \ell_B$ in the initial pulse (Fig. 1a). However the damping time for propagating waves in the ions is so short (~ 0.01 yr, see Fig. 1b) that such waves have virtually no effect on the dynamics.⁵ We conclude that, on time scales of practical

⁵Of course, ion magnetosound waves are suppressed by our numerical code, where the ion inertia is

interest, ion motions in a compressive disturbance are the diffusive motions associated with evanescent waves.

Figure 4 describes the same initial disturbance as Figure 3 but for the SC model where grain magnetosound waves are allowed for wavelengths $\sim \ell_B$ (Fig. 2a). In contrast to the preceding example, the initial disturbance gives rise to two symmetric wave packets propagating in the $\pm z$ directions. That the pulse in Fig. 4 is indeed a packet of grain magnetosound waves can be confirmed by computing the propagation speed: the centers of the forward- and backward-propagating pulses travel a distance $\simeq 1.2 \times 10^{15}$ cm between $t_1 = 8.5$ yr (Fig. 4b) and $t_2 = 77$ yr (Fig. 4d). The propagation speed is therefore 5.0 km s^{-1} , in excellent agreement with V_{gms} (Table 3). The packet is also damped at the expected rate. Taking the width of the pulses ($\simeq 2.6 \times 10^{15}$ cm) at time t_2 as a characteristic wavelength, we find from Fig. 2b that the damping time should be $\simeq 92$ yr. Since the initial amplitude of each counterpropagating pulse is $0.05B_0$, the value of B/B_0 at the peak of the pulse should therefore be $\simeq 1 + 0.05 \exp(-77/90) = 1.022$ at t_2 . This is very close to the numerical value, 1.024, for the data in Figure 4d. Finally, the linear analysis for grain magnetosound waves predicts that the magnitude of the grain velocity⁶ should obey the relation

$$\frac{|v_g|}{C_n} \simeq \left(\frac{V_{\text{gms}}}{C_n} \right) \left[\left(\frac{|B|}{B_0} \right) - 1 \right] \quad (23)$$

in the limit of weak damping, where C_n is the isothermal sound speed (Table 3). At points near the peaks of the pulses, the numerical data for Fig. 4c and 4d satisfy this relation to better than one percent.

Figure 4 also illustrates the different responses of the various fluids to the compressive disturbance. For example, the neutrals are unable to respond at the frequencies corresponding to length scales $\sim \ell_B$ and act simply as a stationary background. The grain velocity lags somewhat behind the ion velocity (Fig. 4a,c) because the time for the charged grains to respond to the magnetic field variations ($\Omega_g^{-1} = 63$ yr, see Table 2) is not much smaller than the flow time scale ($\lesssim 10^{15} \text{ cm} / 5 \text{ km s}^{-1} = 65$ yr). In fact the grains respond somewhat faster than this because of their attraction to the electron-shielded ion quasiparticles, which are attached to the magnetic field. Thus, the ion and grain motions are becoming synchronous by time $t_2 = 72$ yr (Fig. 4c).

neglected. The smallness of the damping time compared to other dynamical time scales of interest justifies this omission.

⁶The neutral and charged grains behave as a single fluid in our simulations of wave packets because the charge fluctuation time is small compared to the flow time scale ($\sim \ell_B/v$).

Figure 5 describes another Gaussian packet in the SC model, but with a larger width, $\ell_B = 1.1 \times 10^{16}$, that is close to the maximum wavelength for propagating grain magnetosound waves (Fig. 1a). As expected, the motion is largely diffusion of the ion-grain plasma with respect to the neutrals, with some additional effects caused by the presence of Fourier components at wavelengths short enough for propagating grain magnetosound waves. Thus, the magnetic field pulse is more smeared out than the analogous pulse in Fig. 3, and has “rounded shoulders” (compare Figs. 3d and 5d). The damping time scale (~ 330 yr, see Fig. 1b) for the wave modes is much less than the decay time ($\gtrsim 5 \times 10^3$ yr) for the longer-wavelength diffusion modes. Grain magnetosound waves are therefore overwhelmingly damped before wave packets can “break out” of the initial Gaussian pulse. After times comparable to the response time of the neutrals ($\sim \tau_{\text{drag}}^{(\text{n,g})}$, see Table 2) the neutrals acquire small nonzero velocities (Fig. 5c) away from the center of the initial pulse, where a density depression appears (Fig. 5d).

Figure 6 describes an even wider packet with $\ell_B = 2 \times 10^{17}$ cm in the SC model. The width now exceeds the minimum wavelength for (propagating) *neutral* magnetosonic waves (Fig. 1a). At times shorter than $\sim \tau_{\text{drag}}^{(\text{n,g})}$ (Table 3), the velocity of the neutrals lags that of the ion-grain fluid (Fig. 6a,b). At much later times (Fig. 6c,d), the ions, grains, and neutrals behave as a single fluid and packets of neutral magnetosound waves start to propagate in the $\pm z$ directions. Because the neutrals are effectively loaded onto the magnetic field lines on these scales, the signal speed is greatly reduced. The data for Fig. 6 imply a propagation speed of about 0.57 km s^{-1} , close to the neutral magnetosound speed (Table 3).

4. Simulations of Multifluid Shock Waves with Dust

We now consider shock waves, which were simulated as follows. At an initial time, $t = 0$, the flow was assumed to be a J shock propagating in the $+z$ direction, with the jump front located at the left-hand boundary of the domain, $z = 0$. The preshock ($z > 0$) region was assumed to be uniform and static initially with values of the density, magnetic field strength and other variables taken from either the WC or SC model. Initial values of the post-shock ($z < 0$) variables were calculated by choosing some initial shock speed, $v_{\text{s,i}}$, and applying the adiabatic jump conditions (assuming a frozen-in magnetic field) at $z = 0$. The flow at later times was determined using our numerical code. Transmissive boundary conditions were applied at both boundaries to simulate a domain extending to $z = \pm\infty$. Adiabatic flow was assumed and the chemistry was turned off; the effects of cooling and chemistry will be discussed in later papers.

4.1. Dust and the Structure of Steady Shocks

We computed a sequence of steady solutions for increasing shock speed, v_s , by integrating the equations of motion to a steady state. For each speed we computed solutions for both the WC and SC models in order to compare effects of dust in the two cases. Instead of the shock speed, it is useful to characterise the steady solutions by the neutral Alfvén Mach number,

$$M_{\text{nA}} \equiv \frac{v_s}{V_{\text{nA}}}, \quad (24)$$

or the grain Alfvén Mach number,

$$M_{\text{gA}} \equiv \frac{v_s}{V_{\text{gA}}}, \quad (25)$$

where $V_{\text{gA}} = V_{\text{gms}}$ is the grain Alfvén speed. Recall that for a two-fluid (ion+neutral) plasma adiabatic shocks have $v_{\text{crit}} = 2.76V_{\text{nA}}$ (Chernoff 1987) or $v_{\text{crit}} = 1.38 \text{ km s}^{-1}$ for the Alfvén speed adopted here (Table 3). To the extent that our solutions resemble the two-fluid case, we expect C type solutions only for shock speeds much smaller than the speeds ($\gtrsim 10 \text{ km s}^{-1}$) in shocked molecular outflows. Thus, our numerical results bear little resemblance to real shocks: dust physics is the issue of interest here.

In fact we expect the WC solutions to be virtually identical to two-fluid shocks with no dust: except for regions very close to a jump front, the grains should move with the neutrals, and therefore have no role in momentum or energy transfer between the charged and neutral fluids. This is verified by Figure 7. The symbols show velocities computed numerically for a shock with $M_{\text{nA}} = 2.1$ using preshock conditions from the WC model. The smooth curves are the exact solution for a steady, two-fluid shock of the same speed (Chernoff 1987; Smith & Brand 1990c).

Figures 8–11 describe a sequence of steady shocks with Alfvén Mach numbers increasing from $M_{\text{nA}} = 2.1$ to $M_{\text{nA}} = 5.0$. It is difficult to pinpoint the C-J transition in these solutions because J-shocks are weak near the transition point (the compression ratio of the shock is unity precisely at the C-J transition) and because artificial viscosity smears out the J front. However it is apparent from Figs. 8–11 that (i) the transition is at or near $M_{\text{nA}} = 2.76$ for the WC model; and (ii) the transition occurs at or near the *same* M_{nA} value for the SC model. The first result is expected for reasons noted above. The second result occurs because the critical speed, $v_{\text{crit}} \simeq 1.38 \text{ km s}^{-1}$, is smaller than the grain magnetosound speed, $V_{\text{gms}} = 5 \text{ km s}^{-1}$. That is, the transition to J-type flow occurs because the neutrals become too hot, not because the shock speed exceeds any signal speed.

The principal difference between the WC and SC solutions in Fig. 8–11 is that the magnetic precursor is thinner in the SC models. Draine (1980) pointed out that the width of

the precursor is inversely proportional to the rate per unit volume, F , at which momentum is exchanged between the charged and neutral fluids. In the WC models momentum transfer is due almost entirely to ion-neutral scattering. Dust contributes virtually nothing because the grains are almost at rest in the neutral fluid. However, in the SC model grain-neutral scattering actually contributes somewhat more to F than ion-neutral scattering (note that $\tau_{\text{drag}}^{(n,g)} < \tau_{\text{drag}}^{(n,i)}$ in Table 2), and this makes the precursors thinner.

We conclude that the signal speed in the grain fluid has no effect on the C-J transition for adiabatic shocks if $V_{\text{gms}} > 2.76M_{\text{nA}}$. We say that C shocks are “cooling limited” in this regime. To explore the regime $V_{\text{gms}} < 2.76M_{\text{nA}}$, we constructed a “heavily loaded” (HL) grain model identical to the SC model (i.e., the grains are well coupled to the field) but with an extremely large dust-to-gas mass ratio, $\rho_{\text{g}}/\rho_{\text{n}} = 0.5$, chosen to make $V_{\text{gms}} = 0.71 \text{ km s}^{-1}$. Figure 12 shows a sequence of steady shocks with increasing speeds computed for the HL model. The solutions are C type for $M_{\text{gA}} < 1$ and J type for $M_{\text{gA}} > 1$, as predicted by Chernoff (1985). We say that C shocks are “signal limited” in this regime, since the C-J transition occurs when v_{s} exceeds the signal speed ($=V_{\text{gms}}$) in the charged fluid. Notice that the ions are forced to move with the grains in these models, since both are coupled to the magnetic field. Consequently there is no magnetic precursor in any fluid for shocks with $M_{\text{gA}} > 1$.⁷

4.2. Dust and the Formation of Magnetic Precursors

Our study of small-amplitude disturbances shows that the response of charged particles to a short-wavelength disturbance depends dramatically on whether or not the dust is coupled to the magnetic field. It is therefore of interest to study how a magnetic precursor forms in these two different cases. Figures 13 through 15 compare shocks in the WC and SC models for a sequence of increasing times. Except for the grain models, both calculations started with identical initial conditions: J shocks with identical compression ratios at $z = 0$ and uniform, static plasma for $z > 0$. The *steady solutions* for the SC (Fig. 15b) and WC (Fig. 15c) models are similar, consistent with the fact that the steady state has a shock speed $v_{\text{s}} < 2.76V_{\text{nA}}$ (see §4.1). However, the intermediate solutions are dramatically different.

Our linear analysis (§3.1) suggests that differences in the flows might be caused by the different mechanisms for transmitting compressive disturbances in the two cases. Strictly speaking the disturbances in Fig. 13–15 are nonlinear; however the linear analysis should give

⁷The slight offsets in Fig. 12c, d between the velocities of charged and neutral particles is a numerical artifact: they are only one grid zone wide.

a reasonable description of the charged fluids, since $v_i \ll V_{\text{ims}}$ and $v_g \ll V_{\text{gms}}$. We therefore adopt the view that the discontinuity imposed by the initial J shock “excites” modes with all possible wavelengths initially, and interpret the subsequent evolution of the flow in terms of these different modes.

Consider first the WC solution. The earliest times shown (Fig. 13a, c and Fig. 14a) are much smaller than the dynamical response times of the dust ($\Omega_g^{-1} \sim 4100 \text{ yr}$) and the neutrals ($\tau_{\text{drag}}^{(\text{n,tot})} \sim 10^4 \text{ yr}$) so only the modes corresponding to pure ion motions are initially of interest. Since these times are also much *longer* than the damping time for propagating ion magnetosound waves (which are suppressed by our code in any case), the rapid ion motions in Fig. 13a, c correspond to evanescent ion magnetosound waves. To see that this interpretation is correct, recall (§3.1) that evanescent waves correspond to diffusive motions. A linear analysis of the ion equations of motion (Appendix A) shows that the diffusion coefficient for the ions is

$$\mathcal{D}_{\text{ion}} = 4\pi^2 V_{\text{ims}}^2 \tau_{\text{drag}}^{(\text{i,n})}. \quad (26)$$

After a time t we therefore expect the “front” separating accelerated from stationary ions to have propagated a distance

$$z_{\text{front}}(t) = (\mathcal{D}_{\text{ion}} t)^{1/2} \quad (27)$$

upstream from the initial J shock. In fact, the predictions of eq. (27) are in remarkably good agreement with the numerical solution for the WC model (Fig. 16). We conclude that a magnetic precursor forms via ion diffusion when dust is dynamically unimportant.

For early times (Fig. 13a, c), the ions simply diffuse through an almost-stationary background of neutrals and dust. After a few hundred years, these ion motions have compressed the magnetic field sufficiently to make the dynamical response time of the grains ($\sim \Omega_g^{-1} \propto B^{-1}$) less than the flow time. At this point (Fig. 14a) betatron acceleration (Spitzer 1976) starts to drive the grain velocity toward the ion velocity. After another few thousand years the neutrals have responded significantly (Fig. 14c). Thereafter (Fig. 15a, c) the evolution slows as the charged and neutral fluids approach mechanical equilibrium, with magnetic pressure balanced by neutral drag in the charged fluid and ion-neutral drag balanced by thermal pressure in the neutral fluid.

Our conclusion — that a magnetic precursor forms via ion diffusion rather than wave propagation when the dust is dynamically unimportant — has important implications. Evidently the conventional wisdom, that the ion magnetosound speed sets an upper limit on v_{crit} when neutral cooling is strong, is incorrect. The upper limit in this situation must occur when the diffusion time scale becomes smaller than the time for ion-neutral scattering to accelerate the neutral gas. An important objective of our future work is to determine

whether this upper limit constrains real shocks with a spectrum of dust sizes and molecular cooling.

Now consider the SC solution. Comparing $z_{\text{front}}(t)$ for the SC and WC models (Fig. 16), we see that the dynamics of the magnetic precursor are *qualitatively different* in the two cases. At very early times there is evidence for “ $t^{1/2}$ behavior” in the SC model (e.g., the curve in Fig. 16 is concave down for small times and the slope is very large near $t = 0$). We attribute this early time behavior to diffusive motions in the ion fluid, which is not strongly coupled to the grains for $t \ll \Omega_g^{-1}$. At later times, $z_{\text{front}} \approx V_{\text{gms}} t$ is a good approximation for the SC model. Clearly, the magnetic precursor forms in the SC model via the propagation of grain magnetosound waves. Now there is a well-defined signal speed, V_{gms} , and it is correct to say that $v_{\text{crit}} = V_{\text{gms}}$. Of course, this is precisely what we found in Fig. 12.

It is of interest to note that a steady C shock forms at an earlier time in the SC model ($\approx 5 \times 10^4$ yr, Fig. 15a) than in the WC model ($\approx 2.6 \times 10^5$ yr, Fig. 15c). This can be understood for the following reasons: First, in the SC model, ions and grains move together and collide in parallel (i.e., simultaneously) with the neutrals. This gives a net collision or momentum-exchange time $\tau_{\text{drag,SC}}^{(\text{n,tot})} = \tau_{\text{drag}}^{(\text{n,g})} (1 + \tau_{\text{drag}}^{(\text{n,i})} / \tau_{\text{drag}}^{(\text{n,g})})^{-1}$ (e.g., see eq. [18]). For the WC model, only collisional drag between ions and neutrals is important, and $\tau_{\text{drag,WC}}^{(\text{n,tot})} = \tau_{\text{drag}}^{(\text{n,i})}$. Inserting the values listed in Table 2, we have $\tau_{\text{drag,SC}}^{(\text{n,tot})} / \tau_{\text{drag,WC}}^{(\text{n,tot})} = 0.4$. Hence, the collisional effect of the ions and grains acting in concert results in momentum transfer that more rapidly “sweeps up” the pre-shocked neutrals in the SC model compared to that which occurs in the WC model. Secondly, the driving mean magnetic field gradient in the precursor region in the SC model is greater than in the WC model. As discussed above, this is due to the difference in the precursor formation mechanism between these models. Rapid ion diffusion disperses the magnetic field ahead of the shock in the WC model over a much larger region than in the SC model (Figs. 15a, c). Because the mean field gradient on the plasma is greater in the SC model than in the WC model, the neutrals thereby also experience a greater accelerating frictional force due to the larger gradient in plasma velocities occurring over a much shorter lengthscale. Thus, taken together, the combined effects of greater momentum transfer by collisions in a more narrowly confined magnetic precursor allows a steady C shock to form at a significantly earlier time in the SC model than in the WC model.

4.2.1. Discussion

For the SC model, which has a population of single-size grains with radius $a_g = 0.05 \mu\text{m}$ and Hall parameter $\Gamma_g = 4.2$, the grain magnetosound speed (eq. [10]) has the typical value

$$V_{\text{gms}} \simeq 5 \left(\frac{B}{50 \mu\text{G}} \right) \left(\frac{2 \times 10^4 \text{ cm}^{-3}}{n_n} \right)^{1/2} \left[\frac{10^{-2}}{(\rho_g / \rho_n)} \right]^{1/2} \text{ km s}^{-1}. \quad (28)$$

However, the single-size grain model that we have assumed here is an idealization to the interstellar medium; in actuality, grains have a distribution in grain sizes, normally spanning more than several orders of magnitude in radii. The very large grains in such a distribution will have $\Gamma_g < 1$ and will therefore not be coupled to the magnetic field (as in the WC model), while the smaller grains will instead have $\Gamma_g > 1$ and will be attached to the field (as in the SC model). The relevant question is then, what is the correct dust abundance that should be used to calculate the numerical value of V_{gms} when there is a distribution in grain sizes?

A likely answer to this question is that one should use the fraction of the charged dust⁸ in the distribution that is coupled to the magnetic field. Neglecting grain-quasiparticle interactions, this corresponds to grains with $\Gamma_g \gtrsim 1$. That the criterion $\Gamma_g \simeq 1$ is the proper one for determining whether charged grains are attached to the magnetic field can be seen in Figures 17*a, b*, which show C shock results for two “intermediately coupled” models, IC-1 and IC-2, respectively. The two models have the same physical parameters as in the WC and SC models (including ion abundances), except that they contain different sized grains: IC-1 has grains with $a_g = 0.125 \mu\text{m}$ and $\Gamma_g = 1.1$, while IC-2 has grains with $a_g = 0.09 \mu\text{m}$ and $\Gamma_g = 1.3$. The initial conditions for the shock flow are the same as for the SC and WC models in Figs. 13 - 15. As in the other models, a steady C shock eventually forms: in IC-1 this occurs at 1.70×10^5 yr, while in IC-2 it is at 1.25×10^5 yr. Comparison of these models with the WC and SC models (Figs. 15*a, c*) shows that, even though the coupling of the grains to the magnetic field in the IC-1 and IC-2 models is not perfect, the shock structure has been significantly altered from that which occurs in the uncoupled WC model. Notably, the grains are moving with the ions and field throughout most of the precursor region in the IC models, and the width of the precursor is substantially smaller than in the WC model. From this, we suggest that the criterion $\Gamma_g = 1$ can reasonably be used to separate grains with a continuous distribution of sizes into two distinct sub-populations of coupled ($\Gamma_g \gtrsim 1$) and uncoupled ($\Gamma_g < 1$) charged grain fluids.

The demarcation between these two sub-populations occurs at the maximum radius of flux-freezing in the grains, $a_{\text{g,fr}}$, which is defined as the radius a_g for which $\Gamma_g = 1$. From

⁸It is assumed here that a non-negligible fraction of the grains are charged (see Table 2); this would also encompass grain models containing a population of very small grains for densities $\lesssim 10^7 \text{ cm}^{-3}$ (e.g., Nishi, Nakano, & Umebayashi 1991; see, also Fig. 1 of Paper I). As noted in § 1, rapid charge fluctuation and momentum transport between neutral and charged grain fluids can effectively couple even the neutral grains to the magnetic field (PHHM87; CM89; Ciolek & Mouschovias 1993). If, however, there is still an extant, non-negligible population of PAHs at these densities, the overall fraction of charged grains may be greatly reduced, with a corresponding increase in V_{gms} (Flower & Pineau des Forêts (2003)).

equation (1) it follows that

$$a_{g,\text{fr}} = 1.0 \times 10^{-5} \left(\frac{B}{50 \mu\text{G}} \right)^{1/2} \left(\frac{2 \times 10^4 \text{ cm}^{-3}}{n_n} \right)^{1/2} \left(\frac{10\text{K}}{T} \right)^{1/2} \text{ cm}. \quad (29)$$

Grains with $a_g \leq a_{g,\text{fr}}$ have $\Gamma_g \geq 1$; to calculate the mass fraction of grains contained in this sub-population, we use the well-known MRN grain distribution function, $f(a_g) \propto a_g^{-3.5}$ (Mathis, Rumpl, and Nordsieck 1977). Using this distribution function, the mass fraction of grains with $a_g \leq a_{g,\text{fr}}$ is

$$\frac{\rho_g(a_g \leq a_{g,\text{fr}})}{\rho_g} = \left(\frac{a_{g,\text{fr}}}{a_{g,\text{max}}} \right)^{1/2} \frac{\left[1 - (a_{g,\text{min}}/a_{g,\text{fr}})^{1/2} \right]}{\left[1 - (a_{g,\text{min}}/a_{g,\text{max}})^{1/2} \right]}, \quad (30)$$

where $a_{g,\text{min}}$ and $a_{g,\text{max}}$ are the minimum and maximum grain radii of the distribution. For our cloud/core models we may take $a_{g,\text{min}} = 0.01 \mu\text{m}$, $a_{g,\text{max}} = 0.3 \mu\text{m}$, which yields $\rho_g(a_g \leq a_{g,\text{fr}}) \simeq 0.48 \rho_g$. Hence, if we replace ρ_g with $\rho_g(a_g \leq a_{g,\text{fr}})$ to estimate the grain magnetosound speed (eq. [10]) in interstellar plasma with a distribution of grain sizes, V_{gms} is only slightly greater than that predicted by equation (28), $\approx 7 \text{ km s}^{-1}$ — which is still considerably lower than the values of v_{crit} determined in the previously noted studies of “cooling limited” shocks. It is possible, then, that the existence and effects of a “signal-limiting” speed V_{gms} on the formation of shocks and magnetic precursors described in this paper will not only be qualitatively but also quantitatively correct even when there is a spectrum of grain radii. As stated above, we hope to definitively resolve this particular issue in future work.

5. Summary

The principal results of this paper are as follows:

1. We calculated the dispersion relations for compressive waves in a dusty plasma for two models, where the dust is weakly coupled and strongly coupled to the magnetic field, respectively. In the “weakly coupled” (WC) model, the only propagating modes in the charged fluids are ion magnetosound waves at very short wavelengths and neutral magnetosound waves at very long wavelengths. In the “strongly coupled” (SC) model, grain magnetosound waves appear at intermediate wavelengths.
2. We simulated the evolution of small-amplitude, Gaussian wave packets to see how different plasma components respond to disturbances on various length scales. When the

length scales are small enough for decoupling of the charged and neutral particles to occur, the dynamics are dramatically different in the WC and SC models. In the WC model there is no wave propagation as such. Propagating ion magnetosound waves are allowed but strongly damped, and so have virtually no effect on the dynamics. Rapid diffusion of ions and electrons through the neutral gas and dust occurs, and the disturbance decays without propagating. In the SC model, packets of grain magnetosound waves appear, and the disturbance propagates (with weak damping) at the grain magnetosound speed. Because the ions and electrons are tied to the magnetic field, the coupling of grains and magnetic field in the SC model suppresses diffusive ion motions.

3. We simulated steady, adiabatic shock waves to compare the effects of dust in the WC and SC models. The WC model gives shocks that are virtually identical to shocks with no dust: steady shocks are C type for Alfvén Mach numbers $M_{\text{nA}} < 2.76$ and J type with magnetic precursors in the ion-electron fluid for $M_{\text{nA}} > 2.76$. We say that steady, adiabatic C shocks are “cooling limited” in the WC model because the C-J transition occurs when the neutrals become too hot to remain everywhere supersonic.
4. Steady, adiabatic C shocks are also cooling limited in the SC model if $V_{\text{gms}} > 2.76V_{\text{nA}}$. Their structures resemble their WC counterparts, with differences attributable to additional momentum transfer caused by grain-neutral scattering.
5. In the SC model steady, adiabatic C shocks are “signal limited” if $V_{\text{gms}} < 2.76V_{\text{nA}}$. In this case the C-J transition occurs when the shock speed exceeds the grain magnetosound speed, as predicted by Chernoff (1985). Shocks faster than the grain magnetosound speed have no magnetic precursor in any fluid.
6. We simulated time-dependent shocks to see how magnetic precursors form in the WC and SC models. Consistent with our study of small-amplitude disturbances, the dynamics are dramatically different in the two cases. In the WC case, a magnetic precursor forms via diffusion of the ion-electron plasma through the dust and neutrals. In the SC case, the precursor forms via the propagation of grain magnetosound waves.

Our calculations incorporated some very unrealistic assumptions in order to isolate the essential physics: Real grains have a spectrum of sizes and real shocks have chemistry and radiative cooling. Having understood the physics, our next investigation will determine realistic values of v_{crit} by relaxing these assumptions.

This work was supported by the New York Center for Studies on the Origins of Life (NSCORT) and the Department of Physics, Applied Physics, and Astronomy at Rensselaer

Polytechnic Institute, under NASA grant NAG 5-7589. Comments from an anonymous referee are acknowledged with appreciation.

A. Diffusion Coefficient for Ions in the Weakly Coupled (WC) Model

The ion-magnetic field diffusion coefficient can be most easily obtained for this particular model by noting that the diffusion mode has the following characteristics (1) it has effective balance between magnetic forces and ion-neutral collisional drag, and (2) the motions of the neutral and grain fluids are negligible compared to that of the ions. Moreover, as previously noted, we may also (3) neglect the effects of quasiparticles in the WC model. With these simplifying assumptions, the linearized versions of the plasma force (per unit volume) equation and magnetic induction equation are then, respectively,

$$0 = -\frac{B_0}{4\pi} \frac{\partial B}{\partial z} - \left(\frac{\rho_i}{\tau_{\text{drag}}^{(i,n)}} \right)_0 v_i \quad (\text{A1})$$

$$\frac{\partial B}{\partial t} = -B_0 \frac{\partial v_i}{\partial z} \quad (\text{A2})$$

(see eqs. [17] and [9] of Paper I). Solving for v_i from equation (A1) and substituting that into (A2) yields the linearized magnetic field diffusion equation,

$$\frac{\partial B}{\partial t} = \left(\frac{B^2}{4\pi\rho_i} \tau_{\text{drag}}^{(i,n)} \right)_0 \frac{\partial^2 B}{\partial z^2} . \quad (\text{A3})$$

Fourier-analyzing this equation corresponds to the replacement $\partial/\partial t \rightarrow -i\omega$, and $\partial/\partial z \rightarrow ik$. Finally, using $\tau_{\text{damp}} = -1/\text{Im}[\omega]$, $\lambda = 2\pi/k$, $V_{\text{ims}} = V_{\text{iA}} = B_{x,0}/\sqrt{4\pi\rho_{i,0}}$, and equation (4) yields the ion diffusion timescale (9). This can also be written as

$$\tau_{\text{damp}}^{(\text{ims})} = \frac{\lambda^2}{\mathcal{D}_{\text{ion}}} , \quad (\text{A4})$$

where \mathcal{D}_{ion} is the ion-magnetic field ambipolar diffusion coefficient (26).

REFERENCES

- Bergin, E. A., Neufeld, D. A., & Melnick, G. J. 1998, *ApJ*, 499, 777
- Bernstein, M. P., Moore, M. H., Esila, J. E., Sandford, S. A., Allamandola, L. J., & Zare, R. N. 2003, *ApJ*, 582, L25

- Chernoff, D. F. 1985, PhD thesis, University of California, Berkeley
- _____. 1987, *ApJ*, 312, 143
- Chernoff, D. F., McKee, C. F., & Hollenbach, D. J. 1982, *ApJ*, 259, 97
- Chièze, J.-P., Pineau des Forêts, G., & Flower, D. R. 1998, *MNRAS*, 295, 672
- Ciolek, G. E., & Mouschovias, T. Ch. 1989, unpublished (CM89)
- _____. 1993, *ApJ*, 418, 774
- _____. 1994, *ApJ*, 425, 142
- _____. 1995a, *ApJ*, 454, 194
- _____. 1998, *ApJ*, 504, 280
- Ciolek, G. E., & Roberge, W. G. 2002, *ApJ*, 567, 947 (Paper I)
- Draine, B. T. 1980, *ApJ*, 241, 1038
- _____. 1986, *MNRAS*, 220, 133
- Draine, B. T., & McKee, C. F. 1993, *ARA&A*, 31, 373
- Draine, B. T., & Roberge, W. G., & Dalgarno, A. 1983, *ApJ*, 264, 485
- Ehrenfreund, P., & Charnley, S. B. 2000, *ARA&A*, 38, 427
- Flower, D. R., & Pineau des Forêts, G. 1994, *MNRAS*, 268, 724
- _____. 2003, *MNRAS*, 343, 390
- Flower, D. R., & Pineau des Forêts, G., Field, D., & May, P. W. 1996, *MNRAS*, 280, 447
- Flower, D. R., Pineau des Forêts, G., & Hartquist, T. W. 1985, *MNRAS*, 216, 775
- Gudipati, M. S., & Allamandola, L. J. 2003, *ApJ*, 596, L195
- Kaufman, M. J., & Neufeld, D. A. 1996a, 456, 250
- _____. 1996b, 456, 611
- Kulsrud, R., & Pearce, W. P. 1969, *ApJ*, 156, 445
- Mathis, J. S., Rumpl, W., & Nordsieck, K. H. 1977, *ApJ*, 217, 425
- Krügel, E. 2003, *The Physics of Interstellar Dust* (IOP: Bristol)
- Mullan, D. J. 1971, *MNRAS*, 153, 145
- Neufeld, D. A., & Stone, J. M. 1997, *ApJ*, 487, 283
- Nishi, R., Nakano, T., & Umebayashi, T. 1991, *ApJ*, 368, 181
- Pilipp, W., Hartquist, T. W., & Havnes, O. 1990, *MNRAS*, 243, 685

- Pilipp, W., Hartquist, T. W., Havnes, O., & Morfill, G. E. 1987, *ApJ*, 314, 341 (PHHM87)
- Pineau des Forêts, G., Flower, D. R., Aguillon, F., Sidis, V., Sizun, M. 2001, *MNRAS*, 323, 7
- Pineau des Forêts, G., Flower, D. R., & Dalgarno, A. 1988, *MNRAS*, 235, 621
- Roberge, W. G., & Draine, B. T. 1990, *ApJ*, 350, 700
- Rosenthal, D., Bertoldi, F., Drapatz, S. 2000, *A&A*, 356, 705
- Smith, M. D. 1991a, *MNRAS*, 252, 378
- _____. 1991b, *MNRAS*, 253, 175
- Smith, M. D., & Brand, P. W. J. L. 1990a, *MNRAS*, 242, 495
- _____. 1990b, *MNRAS*, 243, 498
- _____. 1990c, *MNRAS*, 245, 108
- Smith, M. D., Brand, P. W. J. L., & Moorhouse, A. 1991a, 248, 451
- _____. 1991b, 248, 730
- Smith, M. D., Eisloffel, J., & Davis, C. J. 1998, *MNRAS*, 297, 687
- Smith, M. D., & Mac Low, M.-M., *A&A*, 326, 801
- Spitzer, L., Jr. 1976, *Comments Ap.*, 6, 177
- Timmermann, R. 1996, *ApJ*, 456, 631
- _____. 1998, *ApJ*, 498, 246
- Tóth, G. 1994, *ApJ*, 425, 171
- Wilgenbus, D., Cabrit, S., Pineau des Forêts, G., Flower, D. R. 2000, *A&A*, 356, 1010

Table 1. Model Parameters

Parameter	Symbol	WC Model	SC Model
Preshock density (cm^{-3})	$n_{\text{n}0}$	2×10^4	2×10^4
Preshock magnetic field (μG)	B_0	50	50
Preshock temperature (K) ^a	$T_{\text{n}0}$	10	10
Cosmic ray ionization rate ^b (s^{-1})	ζ_{CR}	8.4×10^{-19}	1.0×10^{-17}
Dust-to-gas mass ratio	$(\rho_{\text{g}}/\rho_{\text{n}})_0$	10^{-2}	10^{-2}
Grain radius (μm)	a_{g}	0.2	0.05

^aAssigned arbitrarily, i.e., not determined by requiring the preshock gas to be in thermal balance. Assumed the same for all fluids.

^bValues selected so that each model has the same degree of ionization $(n_{\text{i}}/n_{\text{n}})_0 = 3.1 \times 10^{-8}$.

Table 2. Properties of the Preshock Plasma

Quantity	Symbol	WC Model	SC Model
Ion-neutral drag time (yr)	$\tau_{\text{drag}}^{(\text{i,n})}$	1.5×10^{-2}	1.5×10^{-2}
Neutral-ion drag time (yr)	$\tau_{\text{drag}}^{(\text{n,i})}$	4.5×10^4	4.5×10^4
Neutral-grain drag time (yr)	$\tau_{\text{drag}}^{(\text{n,g})}$	1.1×10^5	3.0×10^4
Grain-neutral drag time (yr)	$\tau_{\text{drag}}^{(\text{g,n})}$	1.1×10^3	3.0×10^2
Inverse grain gyrofrequency (yr)	Ω_{g}^{-1}	4083	63
Grain Hall parameter	Γ_{g}	0.26	4.2
g^- abundance ^a	x_{g^-}	3.7×10^{-13}	2.2×10^{-11}
g^0 abundance	x_{g^0}	2.2×10^{-14}	2.7×10^{-12}
g^+ abundance	x_{g^+}	8.0×10^{-17}	4.8×10^{-15}
Inverse quasiparticle frequency (yr)	Ω_{qp}^{-1}	1.4×10^{-1}	2.3×10^{-3}
Electrostatic wavelength (cm)	λ_{elect}	2.4×10^{15}	4.0×10^{13}

^aFractional abundance relative to neutral particles.

Table 3. Characteristic Speeds

Quantity	Symbol	Value (km s ⁻¹)
Ion magnetosound speed	V_{ims}	860
Grain magnetosound speed	V_{gms}	5.0
Neutral magnetosound speed	V_{nms}	0.56
Neutral Alfvén speed	V_{nA}	0.50
Neutral adiabatic sound speed	C_{ad}	0.25
Neutral isothermal sound speed	C_{n}	0.19

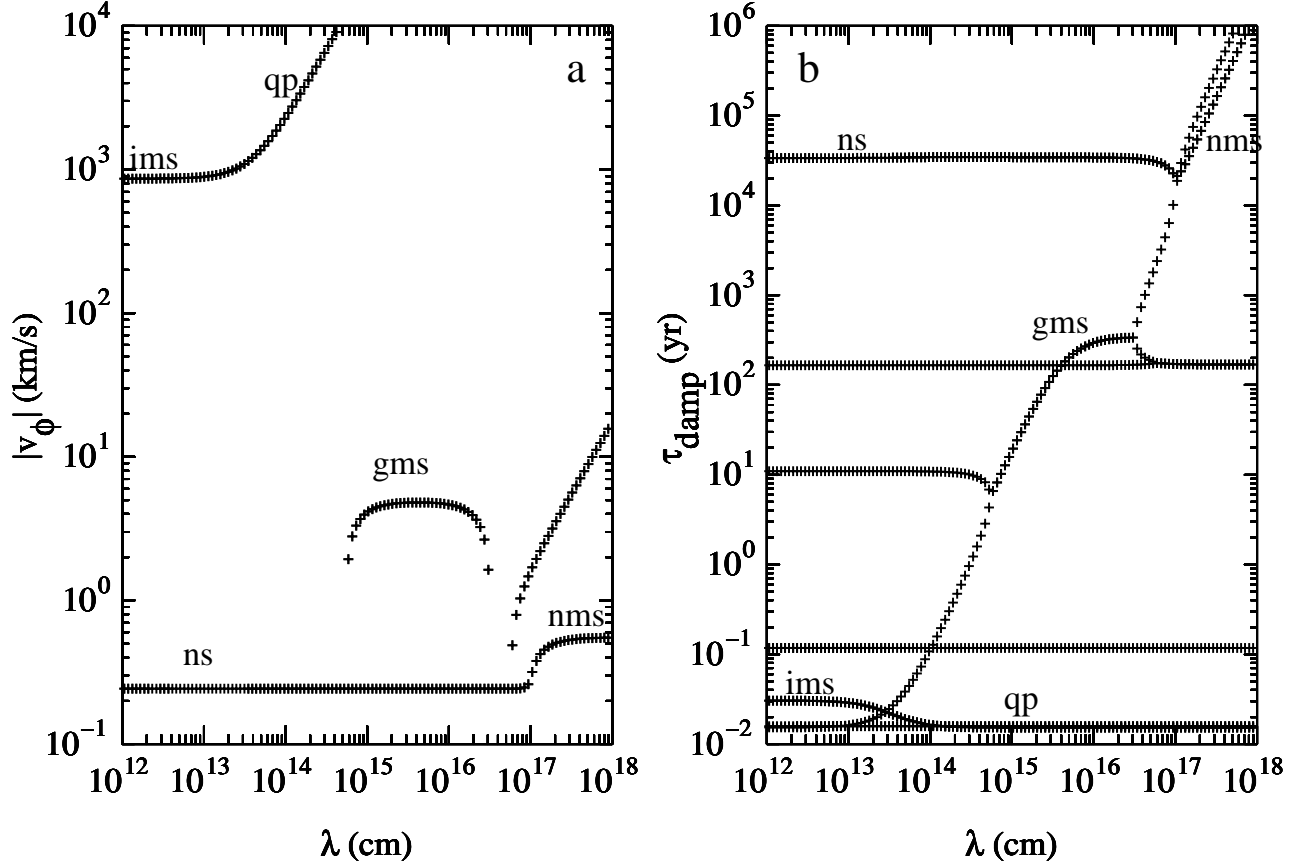


Fig. 1.— Dispersion relation for the WC dust model, where the grains are weakly coupled to the magnetic field. (a) Phase velocity $v_\phi = \omega_r/k$ vs. wavelength, λ , where $\omega_r \equiv \text{Re}[\omega]$ and $k = 2\pi/\lambda$. Various wave modes are labeled. Propagating modes include ion magnetosound (ims), neutral sound (ns), grain magnetosound (gms), and neutral magnetosound (nms) waves. The quasiparticle (qp) mode is a nonpropagating oscillation (see text). (b) Damping time $\tau_{\text{damp}} = -1/\omega_i$, where $\omega_i \equiv \text{Im}[\omega]$. Modes with diffusive damping have a slope $d(\log \tau_{\text{damp}})/d(\log \lambda) = 2$.

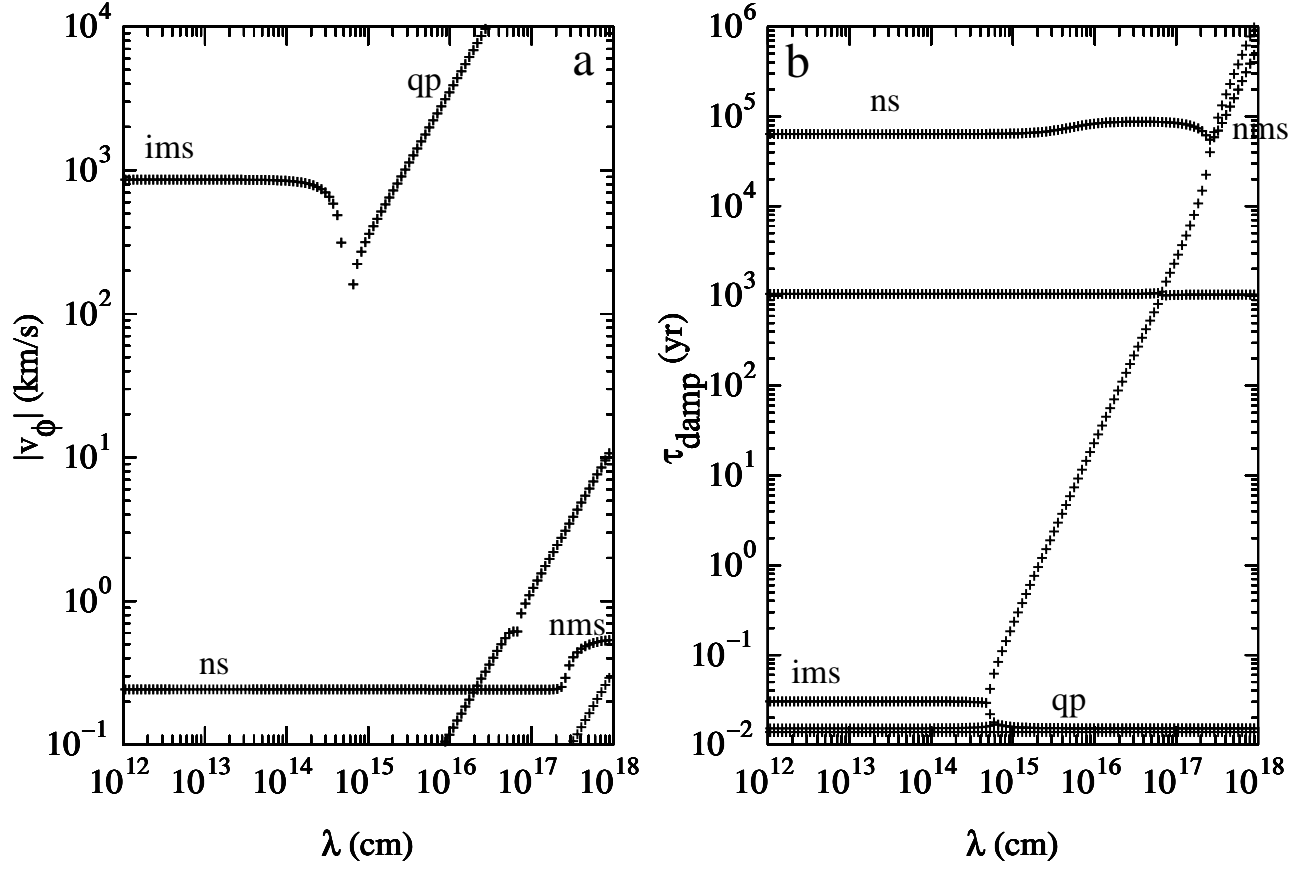


Fig. 2.— Similar to Fig. 1 but for the SC dust model, where the grains are strongly coupled to the magnetic field.

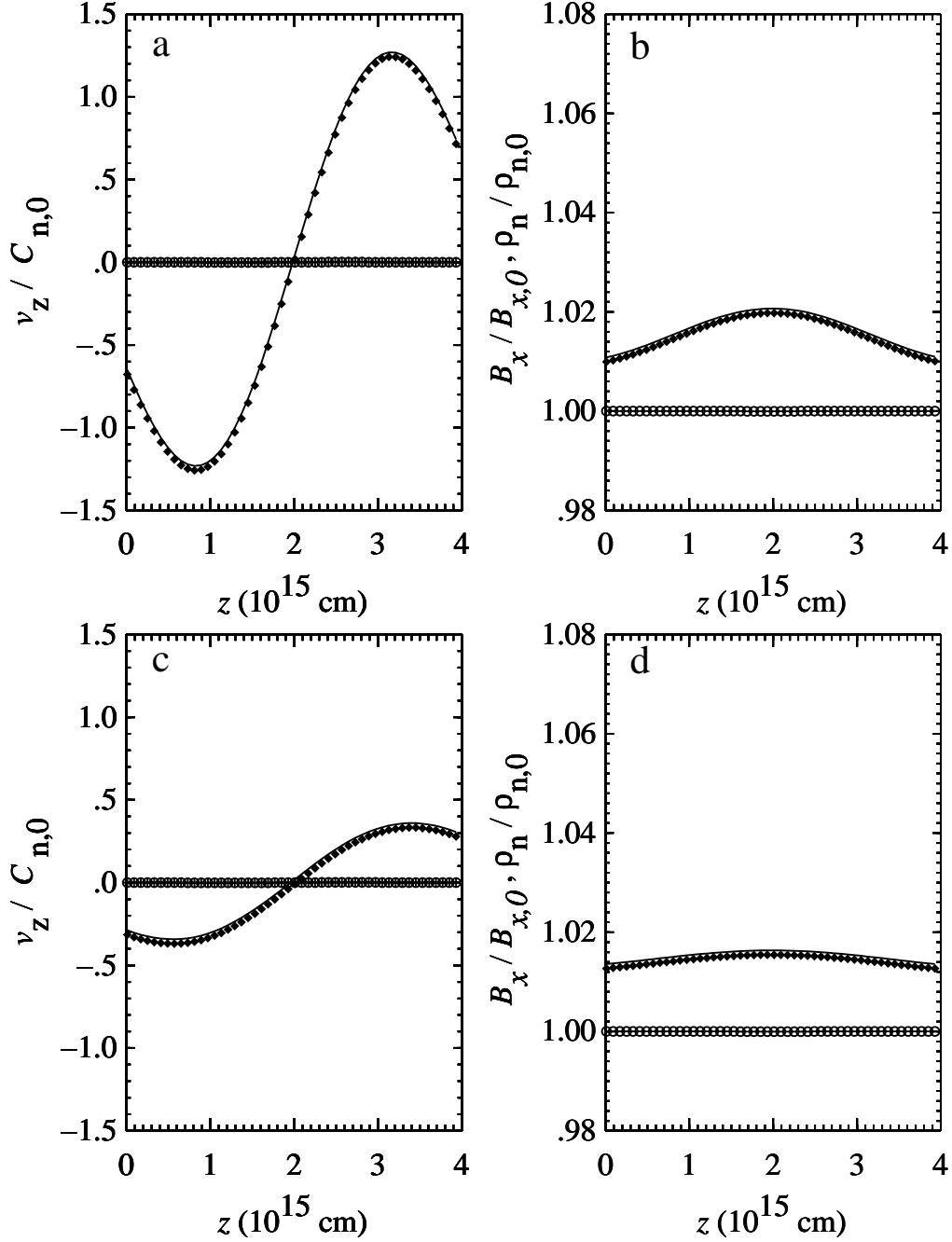


Fig. 3.— Temporal evolution of a Gaussian wavepacket in the WC model. The initial packet width and amplitude are $\ell_B = 4 \times 10^{14}$ cm and $\delta B = 0.1B_0$, respectively. For visual clarity, only every fourth data point is plotted. (a) Velocities of the ions (*filled diamonds*), dust grains (*crosses*), and neutrals (*open circles*) at time $t_1 = 8.5$ yr. Velocities are in units of the isothermal sound speed of the undisturbed state ($= 0.19$ km s $^{-1}$). (b) Magnetic field (*filled diamonds*) and neutral density ρ_n (*open circles*) at time t_1 , normalized to values for the initial undisturbed state. (c) Same as (a) but at a later time $t_2 = 17$ yr. (d) Same as (b), but at time t_2 .

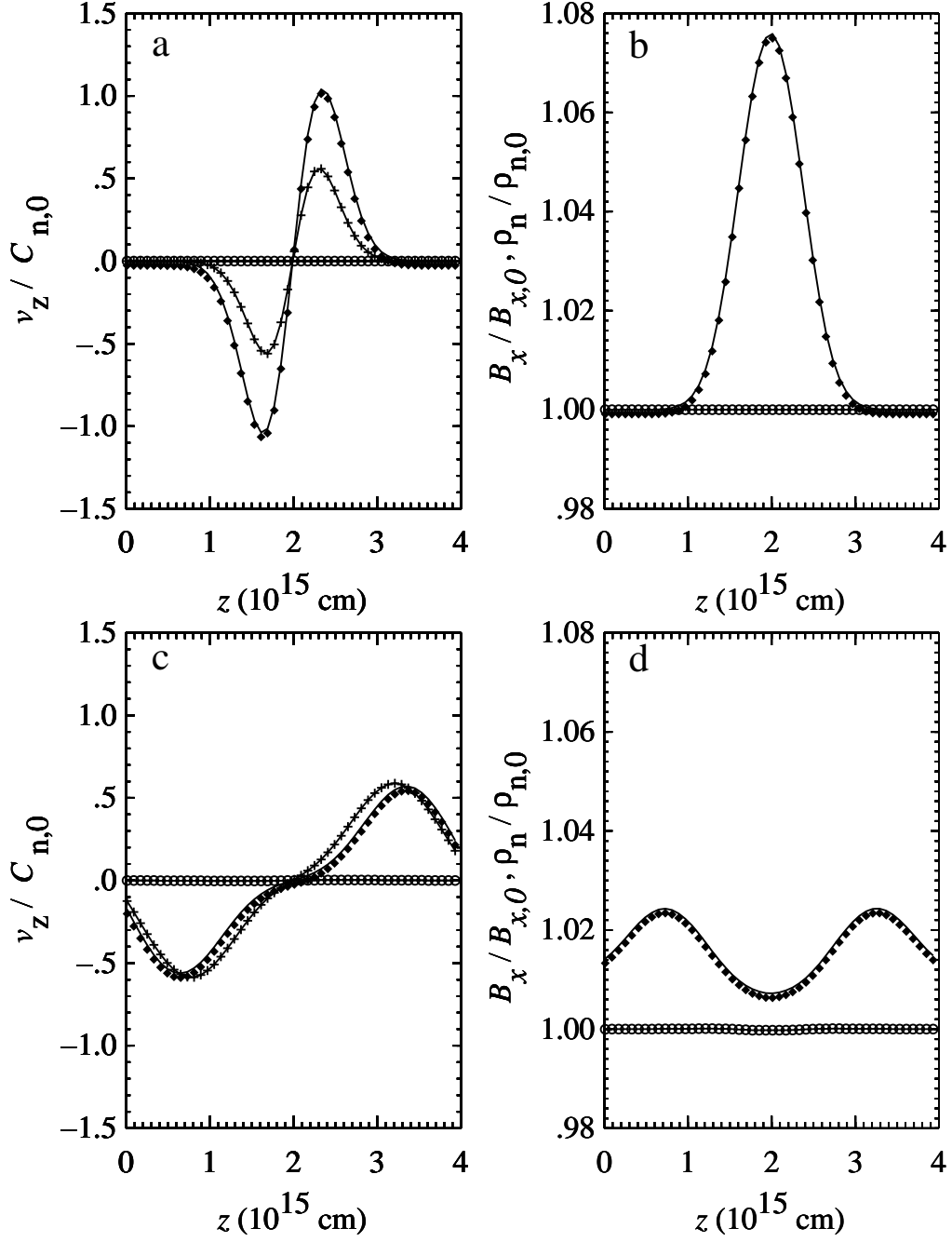


Fig. 4.— Same initial conditions as Fig. 3 but computed for the SC model. (a) Velocities at time $t_1 = 8.5$ yr. (b) Magnetic field and density at time t_1 . (c) Same as (a) but at time $t_2 = 77$ yr. (d) Same as (b) but at time t_2 .

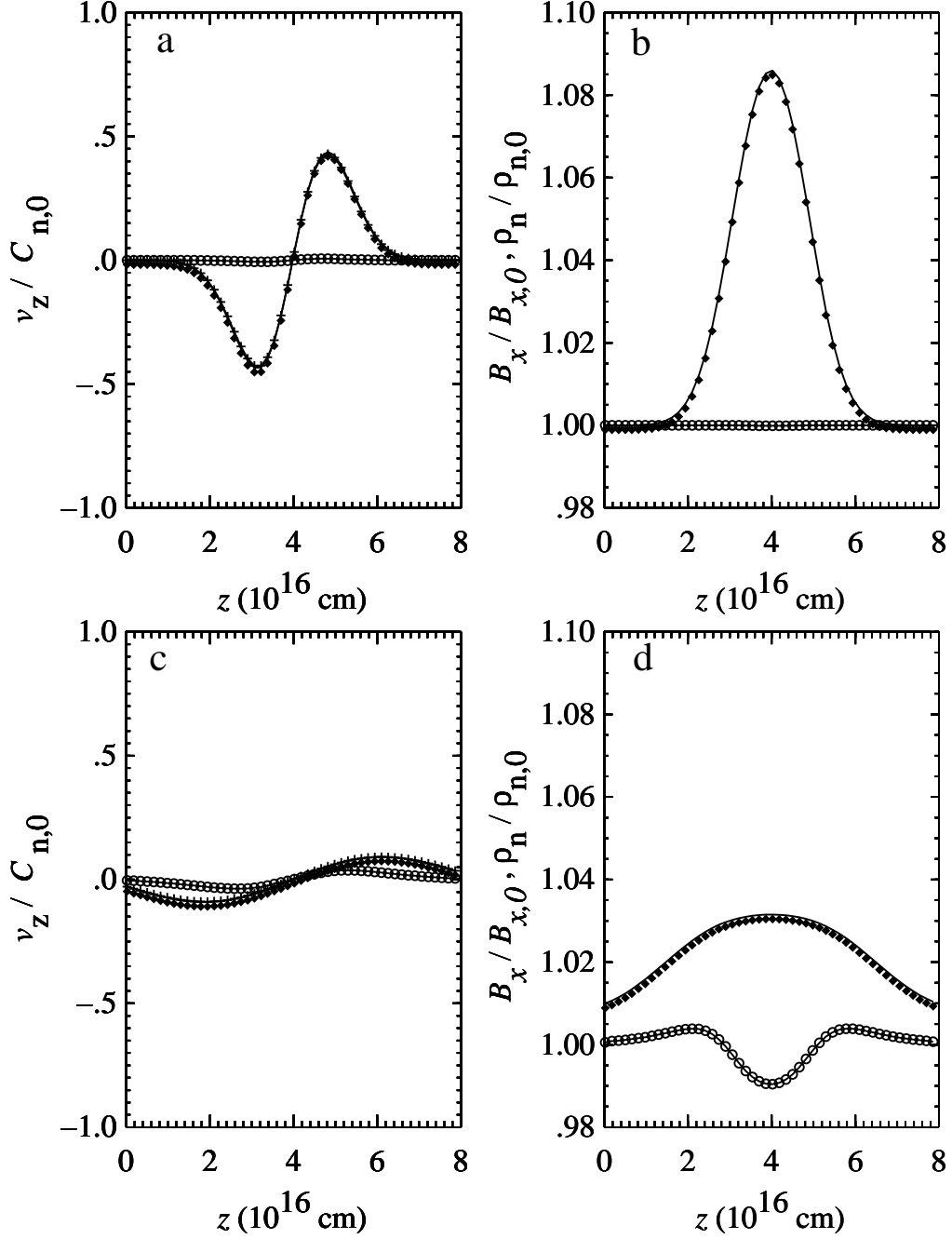


Fig. 5.— Same as Fig. 4 but for a larger initial packet width: $\ell_B = 1.1 \times 10^{16}$ cm. (a) and (b) are at $t_1 = 340$ yr, while (c) and (d) are at $t_2 = 4410$ yr.

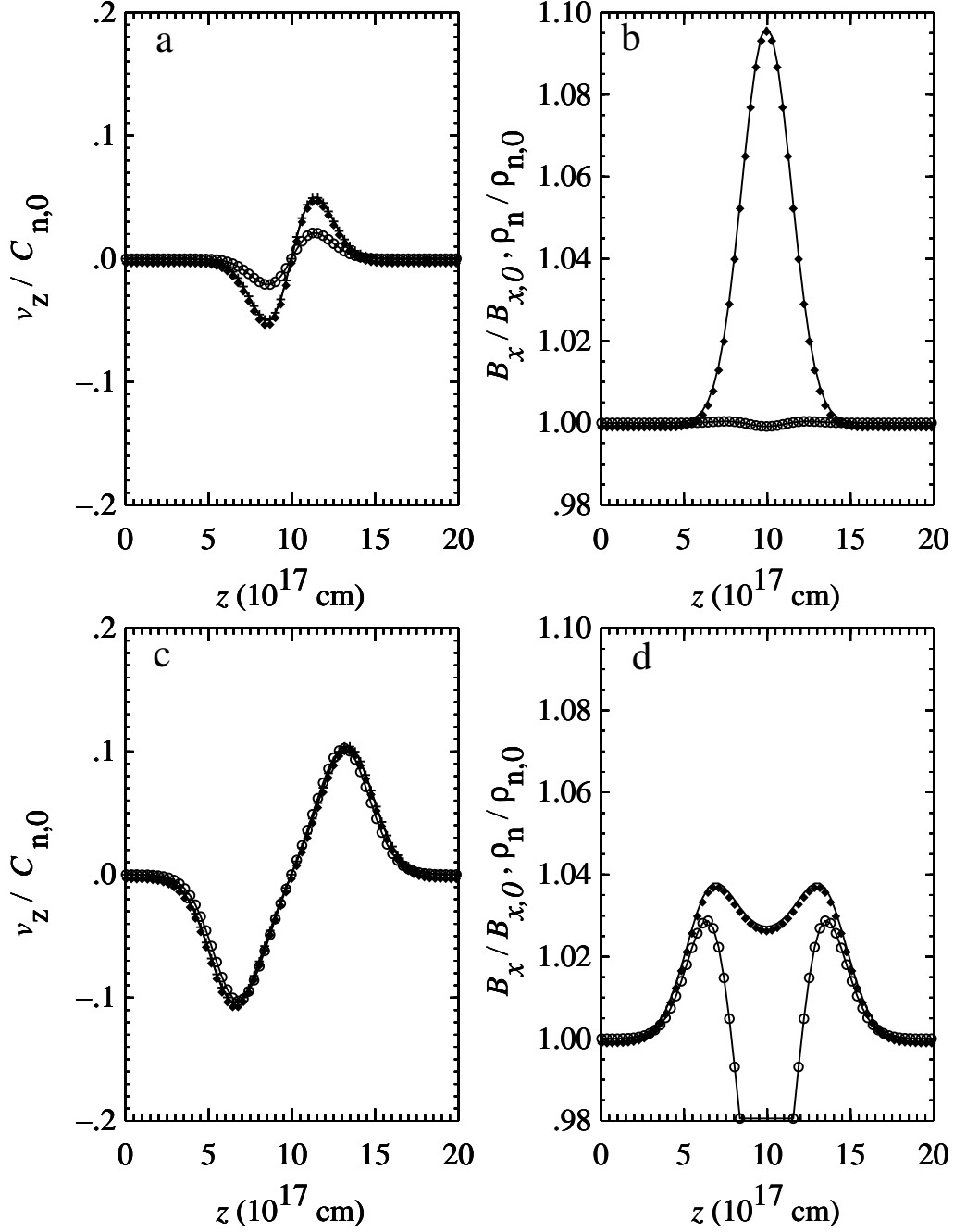


Fig. 6.— Same as Fig. 5 but for an even larger width: $\ell_B = 2 \times 10^{17}$ cm. (a) and (b) are at $t_1 = 1.2 \times 10^4$ yr, while (c) and (d) are at $t_2 = 1.7 \times 10^5$ yr.

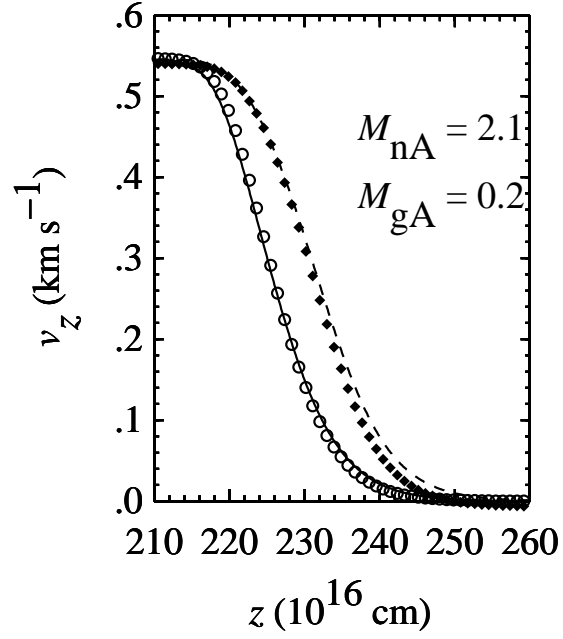


Fig. 7.— Symbols: Numerical predictions of the ion velocity (*filled diamonds*) and neutral velocity (*open circles*) in a steady shock computed for the WC model. Smooth curves: exact solutions for a steady shock with the same speed. The neutral and grain Alfvén Mach numbers are indicated.

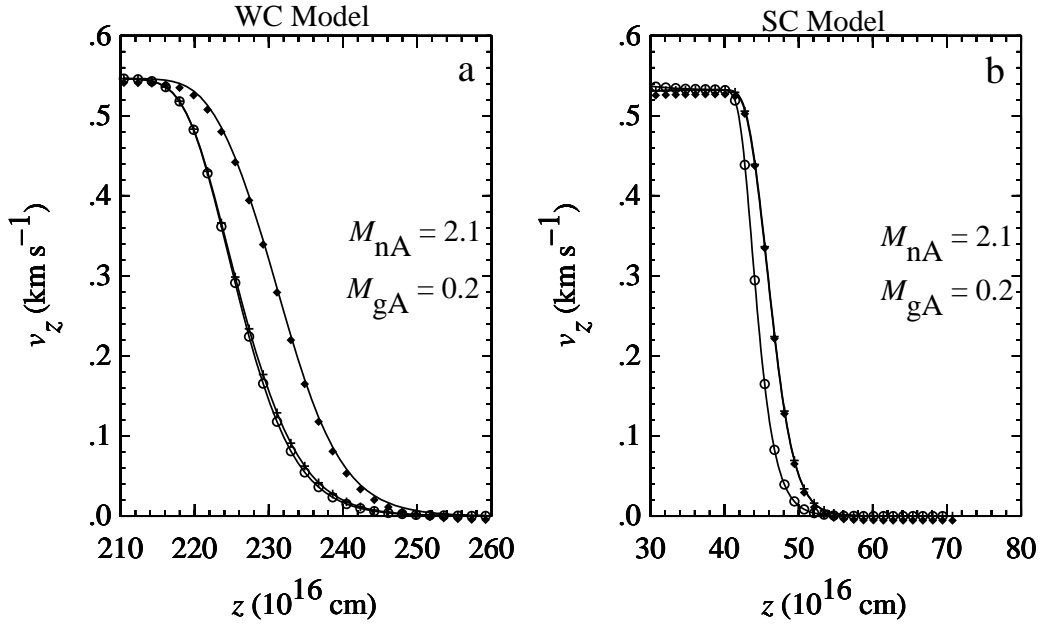


Fig. 8.— Comparison of the velocity profiles for steady, adiabatic shocks with $M_{\text{nA}} = 2.1$ for the WC (Fig. 8a) and SC (Fig. 8b) models. The grain Alfvén Mach number is also indicated. Both solutions are C shocks.

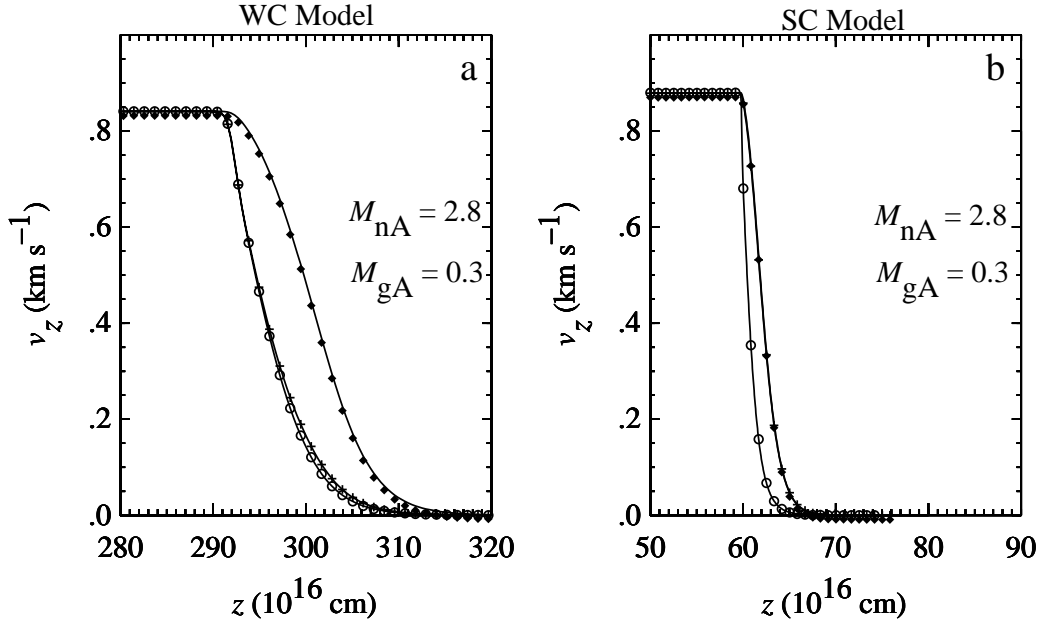


Fig. 9.— Same as Fig. 8 but for $M_{\text{nA}} = 2.8$. Both solutions are weak J shocks. The C-J transition has occurred because the neutral fluid is too hot to remain subsonic.

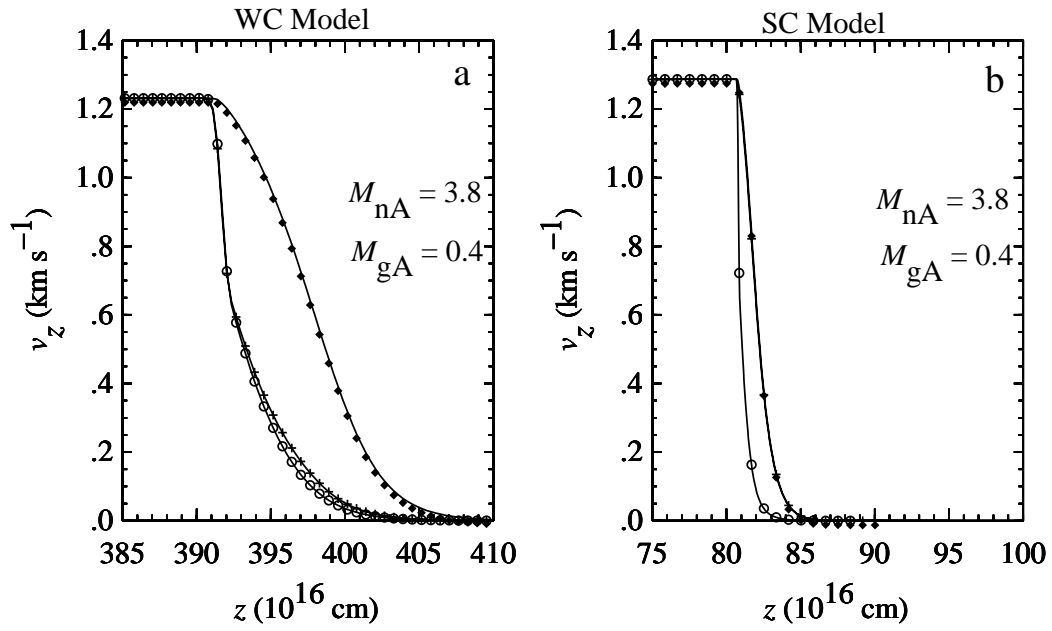


Fig. 10.— Same as Fig. 9 but for $M_{\text{nA}} = 3.8$. In both cases, the solutions are J shocks with magnetic precursors in the charged fluid. In the SC model, the grains move with the ions and electrons. In the WC model, the grains are nearly at rest in the neutral fluid, with a small velocity difference caused by betatron acceleration in the magnetic precursor.

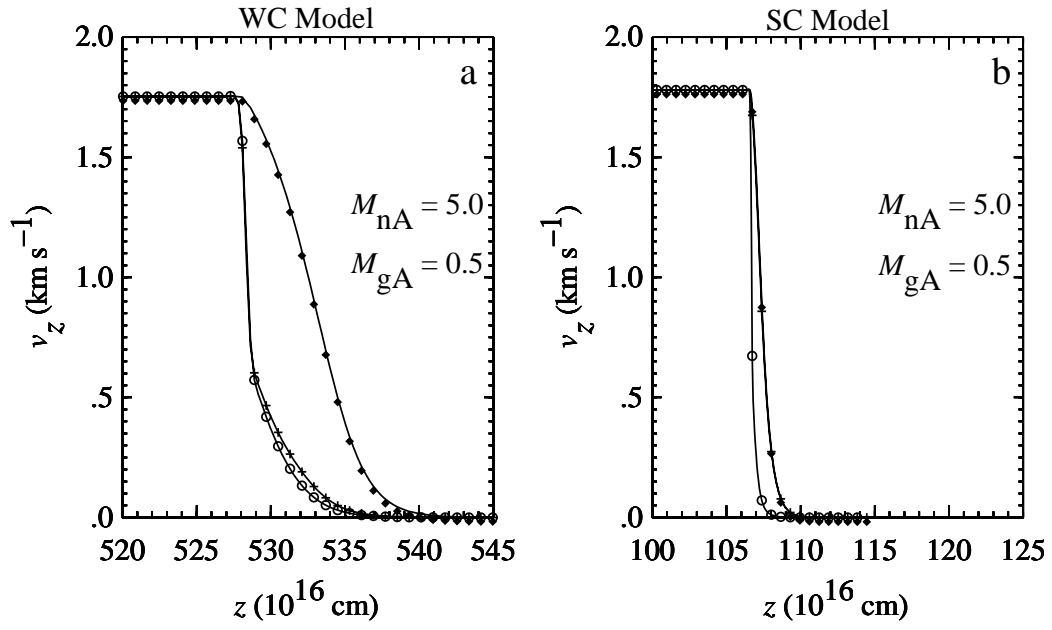


Fig. 11.— Same as Fig. 8 but for $M_{\text{nA}} = 5.0$.

HL Model

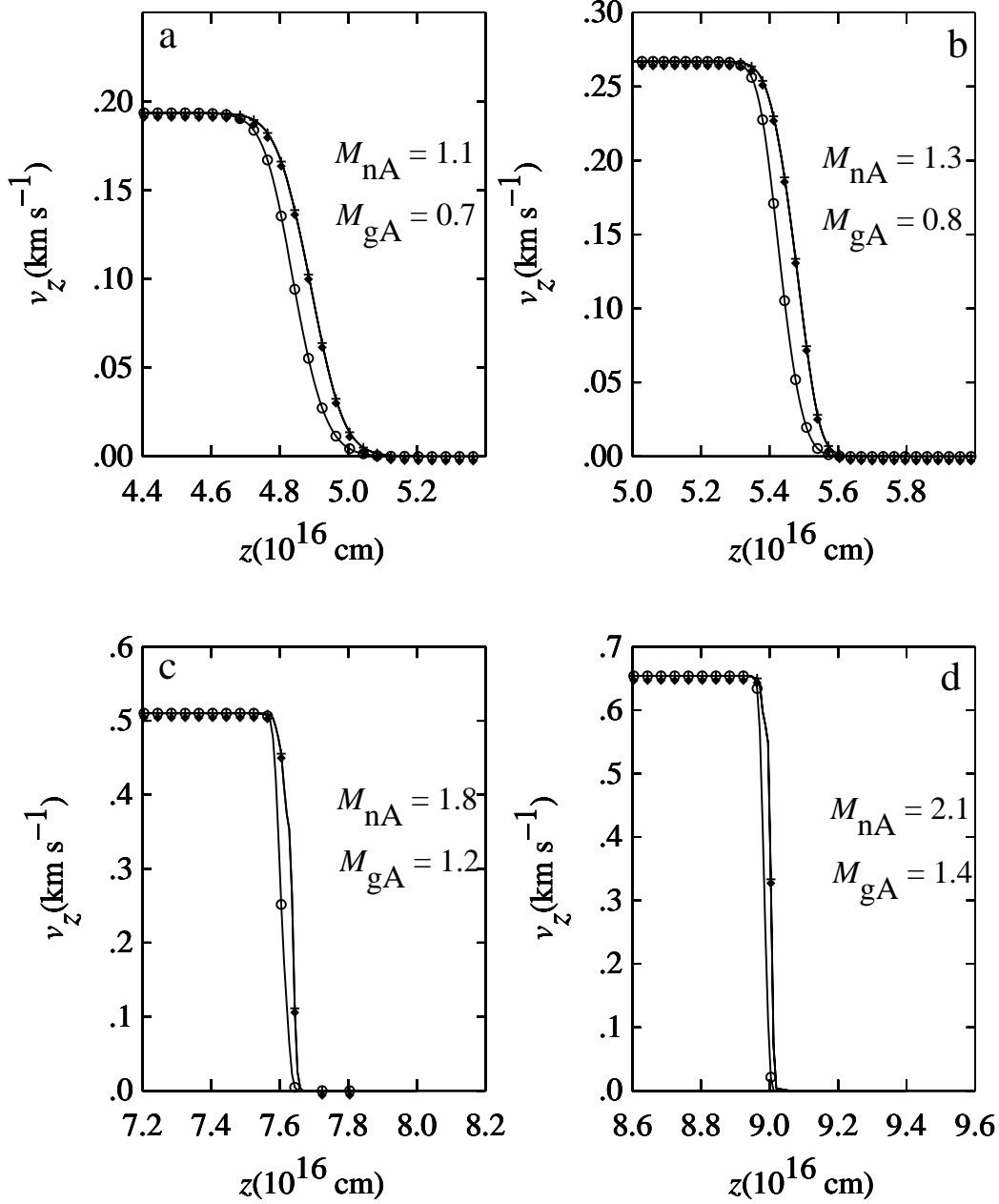


Fig. 12.— Velocity profiles for steady shocks in the “HL” model, where the dust is well coupled to the magnetic field and the grain magnetosound speed is 0.72 km s^{-1} . In this case the C-J transition occurs at $M_{\text{gA}} = 1$, where the shock speed exceeds the signal speed in the charged fluid. Shocks with $M_{\text{gA}} < 1$ (Fig. 12a, b) are C shocks with magnetic precursors in the charged fluid. Shocks with $M_{\text{gA}} > 1$ (Fig. 12c, d) are J shocks with no magnetic precursor in any fluid. (The slight velocity offset between the charged and neutral velocities in Fig. 12c, d is a numerical artifact. See text.)

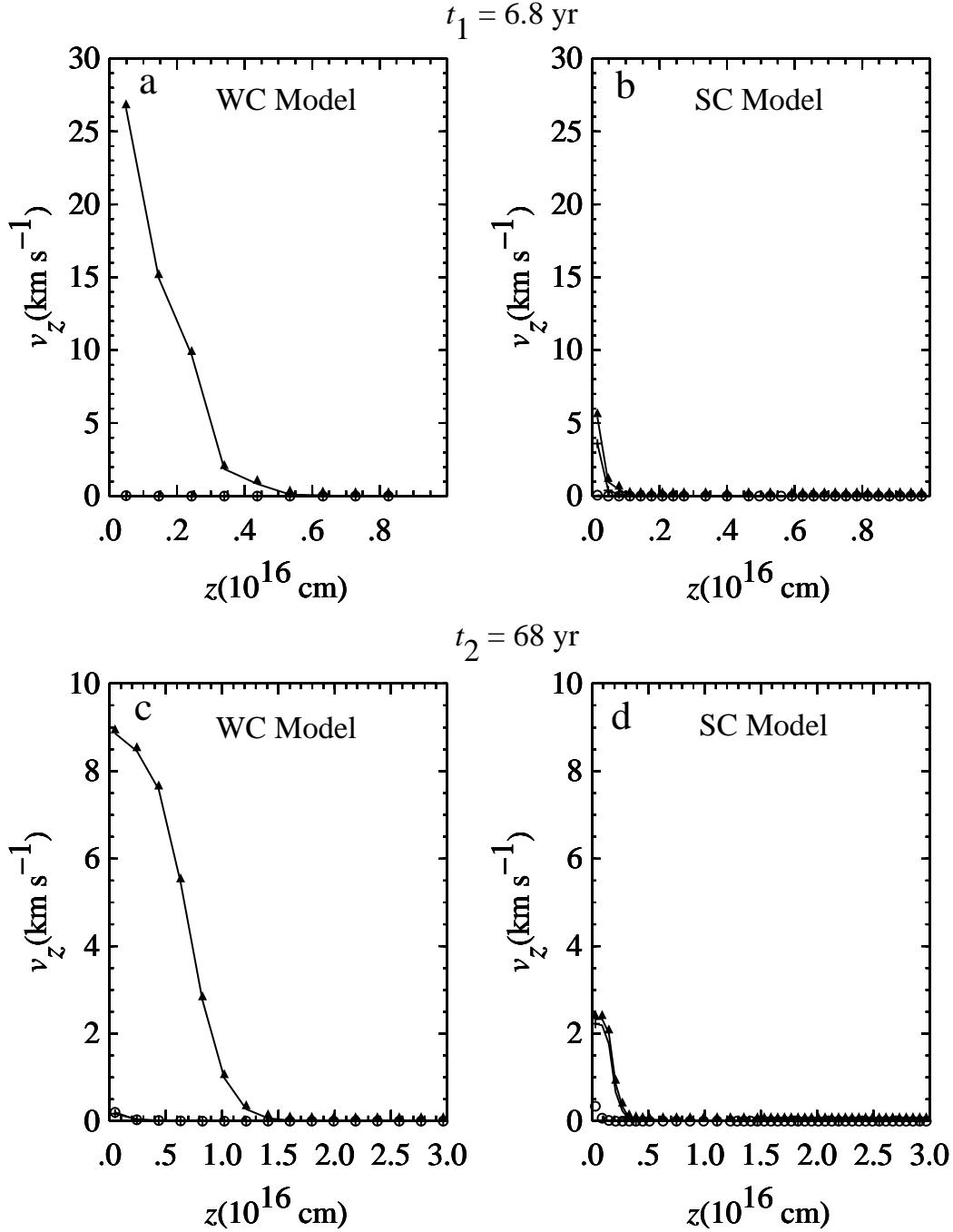


Fig. 13.— Time evolution of a shock in the WC and SC models. At time $t = 0$ the shock discontinuity is located at $z = 0$ and is propagating in the $+z$ -direction. (a) Velocity profile in the WC model at $t = 6.8 \text{ yr}$. (b) SC model at the same time. (c) WC model at $t = 68 \text{ yr}$. (d) SC model at the same time.

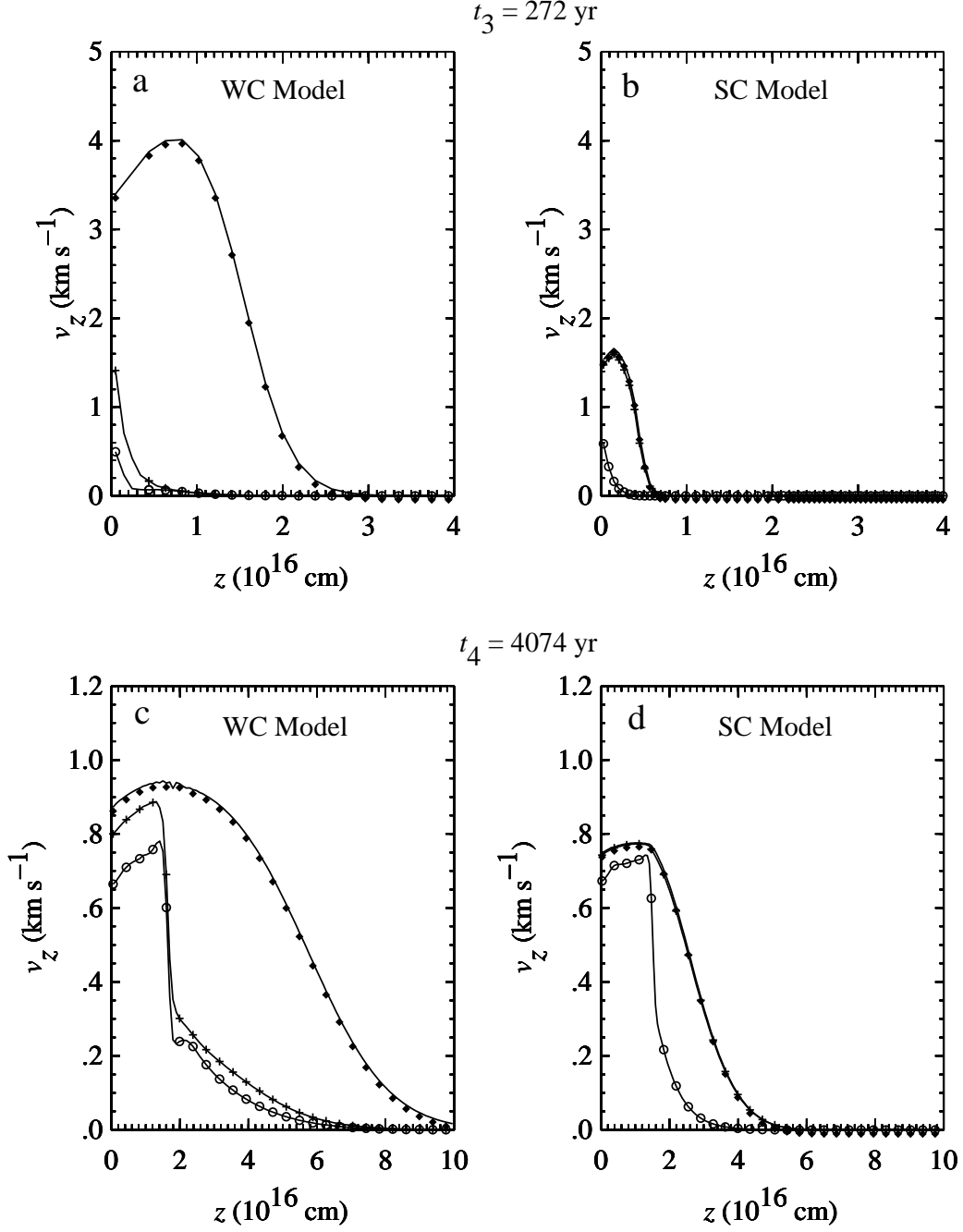


Fig. 14.— Same as in Fig. 13, but at later times. (a) WC model at 272 yr. (b) SC model at the same time. (c) WC model at 4074 yr. (d) SC model at the same time.

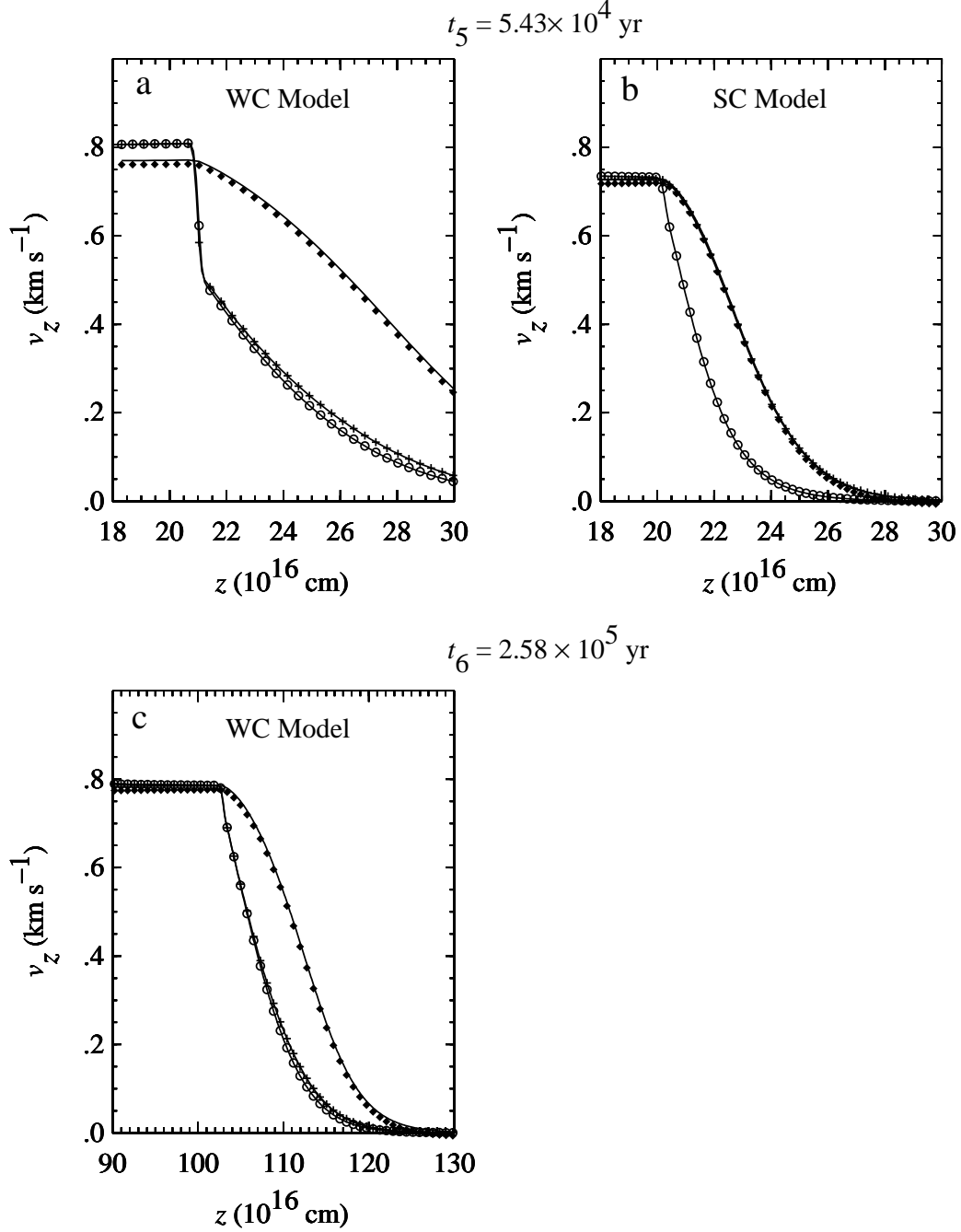


Fig. 15.— Same as in Figs. 13 and 14, but at later times. (a) WC model at $t = 5.43 \times 10^4$ yr. The shock is still in transition, having the characteristics of a J shock with a magnetic precursor. (b) SC model at the same time. By this time, the shock has become a steady C shock. (c) WC model at 2.58×10^5 yr. It is now also a steady C shock by this time. It takes much longer to form a C shock in the WC model than in the SC model because the collisional drag forces (which accelerate the neutrals in the precursor) in the WC model are less than in the SC model.

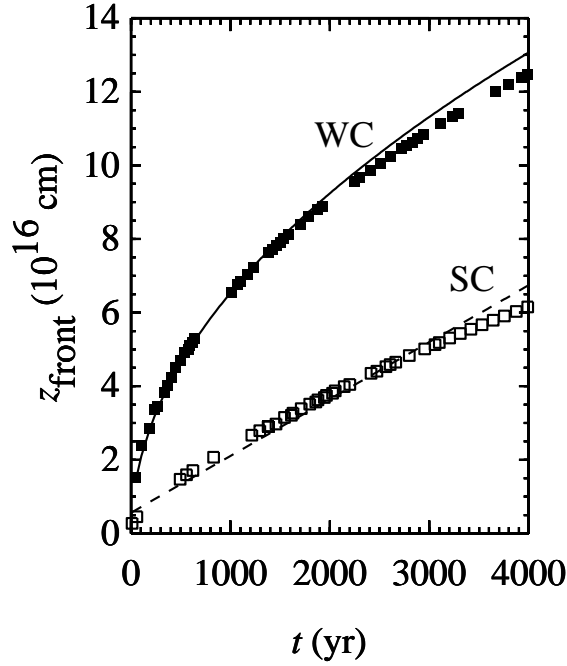


Fig. 16.— Location of the “front” $z_{\text{front}}(t)$ of the hydromagnetic signal that propagates from the initial shock discontinuity at $z = 0$ and $t = 0$ for the WC (*filled boxes*) and SC (*open boxes*) models displayed in Figs. 13 - 15. The location of the front is taken to be the point at which the magnetic field strength B first increases perceptibly ($\approx 0.5\%$) above its preshock (i.e., undisturbed) value. The theoretical prediction of $z_{\text{front}}(t)$ for the ion-diffusion mode ($\propto t^{1/2}$, see eq. [27]) is displayed as the *solid* line. The *dashed* curve corresponds to $z_{\text{front}} = z_{\text{disp}} + V_{\text{gms}}t$, which is the prediction for the grain magnetosound mode, displaced by the amount z_{disp} to coincide with the location of z_{front} at the time $t \approx \Omega_{\text{g}}^{-1}$.

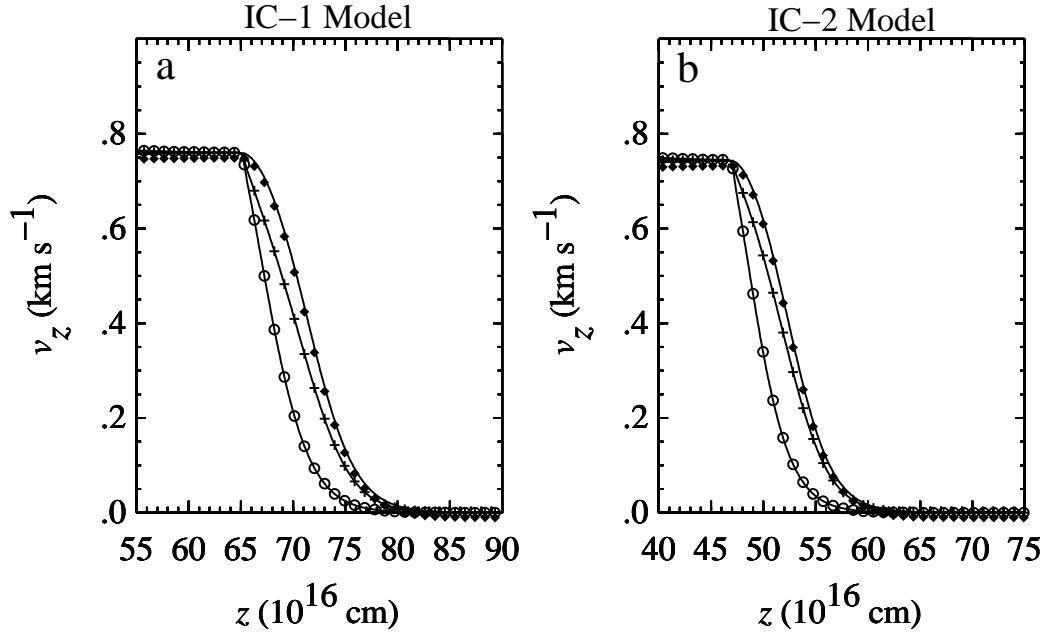


Fig. 17.— C shock flow in “intermediately-coupled” models. The initial shock conditions and physical parameters are the same as for the WC and SC models shown in Figs. 13 - 15, except that the IC-1 model has grains with $a_g = 0.125 \mu\text{m}$ ($\Gamma_g = 1.1$), while IC-2 has $a_g = 0.09 \mu\text{m}$ ($\Gamma_g = 1.3$). (a) IC-1 model when it has a steady C shock at $t = 1.70 \times 10^5 \text{ yr}$. (b) Steady C shock flow in the IC-2 model at $t = 1.25 \times 10^5 \text{ yr}$.